Variation in temperature of peak trait performance will constrain adaptation of arthropod populations to climatic warming

Samraat Pawar[1*], Paul J. Huxley[1,5*], Thomas R. C. Smallwood[2], Miles L. Nesbit[1,3], Alex H. H. Chan[1], Marta S. Shocket[4], Leah R. Johnson[5], Dimitrios - Georgios Kontopoulos[6], Lauren Cator[1*]

[1]Department of Life Sciences, Imperial College London, Silwood Park Campus, Ascot, UK

[2]Department of Infectious Disease Epidemiology, Imperial College London, St Mary's Campus, London, UK

[3] The Pirbright Institute, Woking, UK

[4]Department of Geography, University of Florida, Gainesville, FL, USA

[5]Department of Statistics, Virginia Tech, Blacksburg, VA, USA

[6]LOEWE Centre for Translational Biodiversity Genomics & Secenenberg Research Institute, Senckenberg, Frankfurt, Germany

*To whom correspondence should be addressed; E-mail: s.pawar@imperial.ac.uk, phuxley@vt.edu, l.cator@imperial.ac.uk

The degree to which arthropod populations will be able to adapt to climatic warming is uncertain. Here, we report that arthropod thermal adaptation is likely to be constrained in two fundamental ways. First, maximization of population fitness with warming is predicted to be determined predominantly by the temperature of peak performance of juvenile development rate, followed by that of adult fecundity, juvenile mortality and adult mortality rates, in this specific order. Second, the differences among the temperature of peak performance of these four traits will constrain adaptation. By compiling a new global dataset of 61 diverse arthropod species, we show that contemporary populations have indeed evolved under these constraints. Our results provide

a basis for using relatively feasible trait measurements to predict the adaptive capacity of arthropod populations to climatic warming.

Arthropods are highly diverse and constitute almost half of the biomass of all animals on earth, fulfilling critical roles as prey, predators, decomposers, pollinators, pests, and disease vectors in virtually every ecosystem (*1*). Arthropod populations are under severe pressure globally due to pollution and land use changes, which is likely to be compounded by ongoing and future climate change (*2–5*). The ability of these populations to adapt to climatic warming in particular has far-reaching implications for ecosystem functioning, agriculture, and human health (*6–8*).

The ability of a population to persist—its fitness—depends on its maximal growth rate (r_m, also known as intrinsic growth rate) in a given set of conditions. The response of arthropod r_m to environmental temperature is unimodal, with its peak typically occurring at a temperature (T_{opt}) closer to the upper, rather than to the lower lethal limit (a left-skewed temperature-dependence; Fig. 1A) (*9–11*). This temperature-dependence of r_m emerges from the thermal performance curves (TPCs) of underlying life history traits (Fig. 1B) (*12, 13*). Previous work has focused on the effect of thermal sensitivity (E, Fig. 1B, SM Table 1) (*13, 14*) or upper lethal thermal limit (CT_{max}) (*15–17*) of traits on the temperature-dependence of r_m, providing insights into the responses of populations to short-term thermal fluctuations and heat waves on populations (*18–20*). However, to understand how populations will respond to long-term sustained climatic warming, we need to quantify the adaptive potential of the temperature at which fitness peaks with respect to temperature (T_{opt}) as well as the r_m achieved at that temperature ("thermal fitness"; Fig. 1A). Adaptive shifts in T_{opt} and its associated thermal fitness are primarily governed by shifts in the T_{pk}s of underlying traits (Fig. 1B) (*12, 13*), which can potentially evolve relatively rapidly under selection because they are subject to weaker thermodynamic constraints than thermal sensitivity or CT_{max} (*11, 21, 22*). However, a sufficiently general trait TPC-based approach to quantify the adaptive potential of diverse arthropod populations to climatic warming remains elusive (*8, 19, 23, 24*).

Here, we combine metabolic and life history theories to predict how variation in trait T_{pk}s affect the thermal fitness and potential adaptation of arthropod populations to chronic (directional) changes in temperature. We test our predictions with a global data synthesis representing a diverse set of 61 arthropod taxa. Our analysis reveals two fundamental constraints on adaptation which arise from how TPCs of individual traits combine to determine the temperature-dependence of arthropod population fitness.

The trait-driven temperature-dependence of fitness

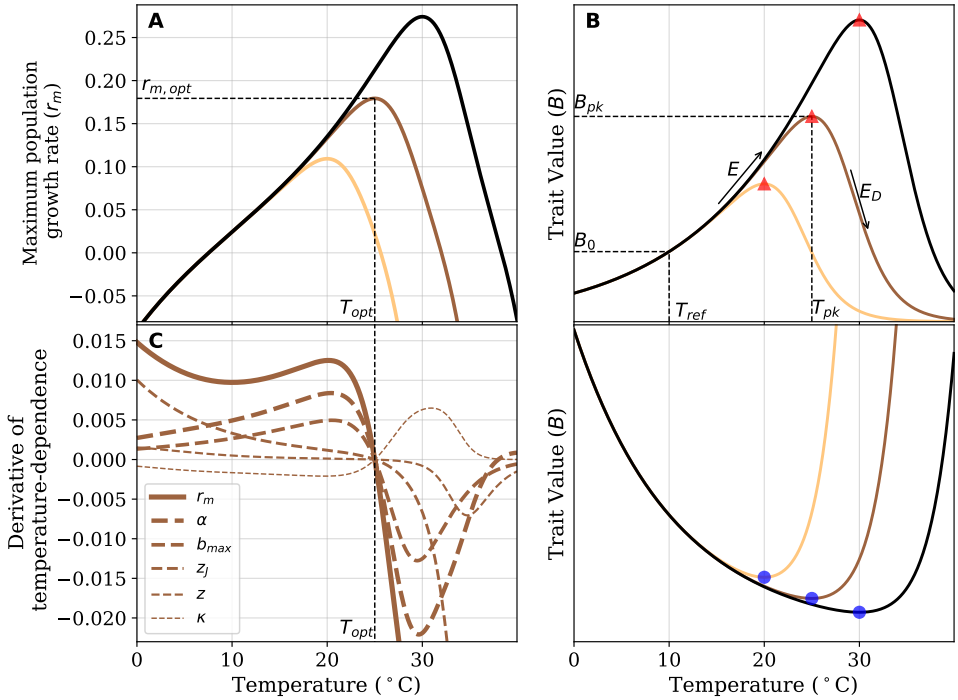

Figure 1: The predicted temperature-dependence of population fitness and underlying traits. In both panels, the three curves represent populations adapted to three different temperatures. **A**: The temperature-dependence of population growth rate r_m (SM Eqn 2). Thermal fitness is the peak value that r_m reaches ($r_{m,opt}$) and T_{opt} the temperature at which this peak is achieved. **B:** *(Upper)* Illustration of the underlying trait TPCs modeled using the Sharpe-Schoolfield equation (SM Eqn 3, SM Table 1), appropriate for development rate $1/\alpha$, maximum fecundity b_{max}, and fecundity decline rate κ. **B:** *(Lower)* Illustration of a trait TPC modeled using the inverse of the Sharpe-Schoolfield equation, appropriate for juvenile mortality rate z_J and adult mortality rate z. B_0 is the normalization constant for the trait value at a reference temperature (T_{ref}) and B_{pk} is the trait performance value at the temperature of peak performance (T_{pk}) (SM Table 1). All sets of curves were generated with arbitrary, but empirically reasonable values for TPC parameters chosen for illustration (SM Materials and Methods). The y-axes values are arbitrary and not shown. **C**: Relative contributions of each trait's TPC to the temperature dependence of r_m. The greater the distance between a trait's partial derivative (dashed curves, i.e., $\frac{\partial r_m}{\partial \theta}\frac{\mathrm{d}\theta}{\mathrm{d}T}$ where θ denotes any one of the five traits) and the total derivative $\frac{dr_m}{dT}$ (solid curve), the smaller its contribution to r_ms temperature dependence.

We started with a mathematical equation for the temperature-dependence of r_m (Fig. 1A; SM Eqn 2) as a function of the TPCs for five key life history traits (Fig. 1) (*12*): juvenile-to-adult

development time, α; juvenile mortality rate, z_J; maximum fecundity, b_{max}; fecundity decline with age, κ; adult mortality rate, z. This simplification of the diverse and complex stage-structures seen in arthropods to five traits allows us to make general predictions that can be applied across taxa. This equation predicts that the temperature-dependence of r_m increases as a population adapts to warmer temperatures (i.e., thermal fitness rises with T_{opt}; Fig. 1A). This "hotter-is-better" pattern is consistent with the findings of empirical studies on arthropods as well as other ectotherms (*10, 25*). In our theory, this pattern arises through thermodynamic constraints on life history traits built into the Sharpe-Schoolfield equation for TPCs (SM Eqn 3), which focuses on a single, rate-limiting enzyme underlying metabolic rate (*26*). While previous theoretical work has sought to understand the evolutionary basis and consequences of the hotter-is-better phenomenon (*10, 15, 19, 22, 25, 27*), to the best of our knowledge, this is the first time that the contributions of underlying traits to it have been quantified.

The existence of a hierarchy of traits driving thermal fitness

We next performed a trait sensitivity analysis to dissect how trait TPCs shape the temperature-dependence of r_m (Fig. 1C). It shows that populations will grow (r_m will be positive) as long as the negative fitness impact of an increase in juvenile and adult mortality rate (z_j and z) with temperature is counteracted by an increase in development and maximum fecundity rate (α and b_{max}). So, for example, r_m rises above 0 at $\sim$9°C (Fig. 1A) because that is around where z_J and z fall below, and α and b_{max} rise above, a particular threshold (Fig. 1C). Similarly, the decline of r_m beyond T_{opt} is determined by how rapidly each of the underlying trait values change with temperature beyond that point (determined by their respective E_Ds). More crucially, the trait sensitivity analysis reveals a hierarchy in the importance of life history traits in driving both the location of thermal fitness (i.e., T_{opt}) and its height (i.e., the thermal fitness achieved) (Fig. 1C): the TPC of development time (α) has the greatest influence followed by maximum fecundity (b_{max}), juvenile mortality (z_J), adult mortality (z) and fecundity loss rate (κ), with each of the latter three having a particularly weak effect $\sim$5°C around T_{opt} (Fig. 1C). It is only at extreme temperatures (Fig. 1C, $T < 10$°C and $T > 35$°C) that juvenile mortality (z_j) in particular exerts a strong influence on the temperature-dependence of r_m. Thus the influence of the five traits in the region of thermal fitness can be ordered as $\alpha > b_{max} > z_J > z > \kappa$. This is expected to be a general result, consistent with the type of stage structure typical of arthropod, and especially insect, populations where the juvenile stages altogether are both more abundant and longer-lived than adults (*19, 20*).

The trait hierarchy shapes thermal fitness

Next we focused on trait T_{pk}s as key targets of selection leading to thermal adaptation, that is, maximization of thermal fitness in a given constant thermal environment. We calculated thermal selection gradients and strengths of selection for each trait's T_{pk} (Fig. 2). For the range of environmental temperatures we consider (0°C to 35°C), T_{opt} varies by about 12°C ($\sim$ 16°C to

28°C). Every trait's thermal selection gradient is necessarily asymptotic because, even if the T_{pk} of that trait keeps increasing with environmental temperature, all traits decline with temperature beyond their respective T_{pk} (Fig. 1B). These calculations predict that selection is strongest on the temperature of peak performance of development time (α), followed by those of the other traits in the same order ($T_{pk}^{\alpha} > T_{pk}^{b_{max}} > T_{pk}^{z_J} > T_{pk}^{z}$), in line with our trait sensitivity analysis (Fig. 1C). We excluded κ from this analysis because it has a very weak influence on r_m (Fig. 1C) and TPC data are also lacking for it (SM Materials and Methods). SM Section 2.7 shows that our results are indeed robust to variation in κ's temperature dependence.

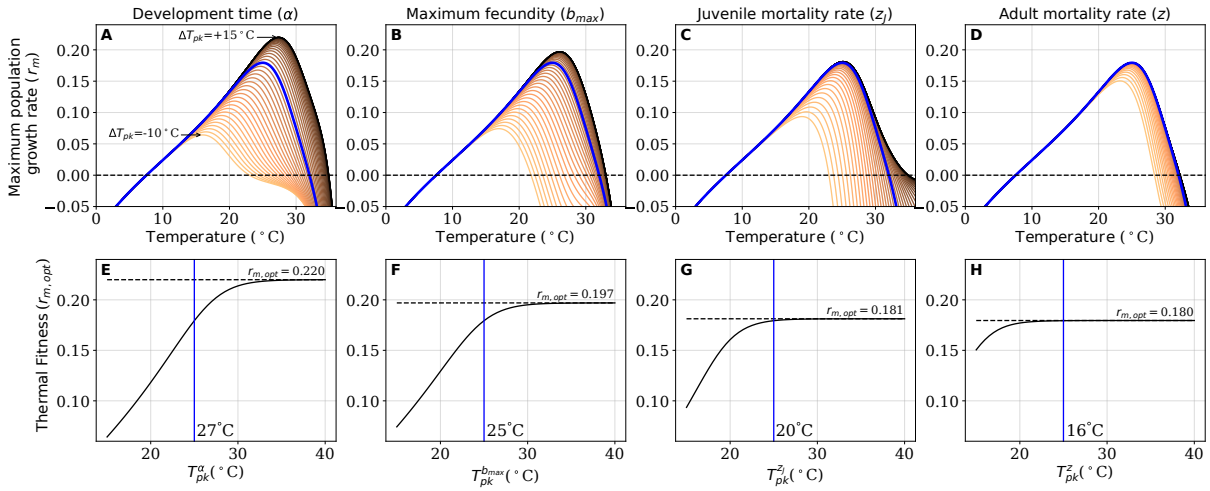

Figure 2: Thermal selection gradients for four key arthropod life-history traits. A-D: Change in the TPC of r_m with changes in T_{pk}s of each of the four traits relative to all the others (ΔT_{pk}). ΔT_{pk} ranges from -10°C (light lines) to $+15$°C (dark lines), solid blue line indicates the scenario in which all traits peak at the same temperature ($\Delta T_{pk} = 0$) **E-H**: The corresponding selection gradients for each trait (SM Materials and Methods). The solid black line represents r_m. The solid blue line represents $\Delta T_{pk} = 0$ and any increase in r_m to the right of this point represents potential increase in fitness that could be gained by increasing the T_{pk} of the trait relative to others. Thus, the optimal T_{pk} of each trait is expected to lie after the asymptote of the gradient is reached. Both sets of plots (A-D & E-H) are ordered by decreasing strength of selection on the trait, that is, in reverse order of the T_{pk} at which minimum of the quantity $\frac{\partial^2 r_{opt}}{\partial {T_{pk}^{\theta}}^2}$ is reached. This quantity measures where the selection gradient begins to asymptote, indicated by the vertical blue line in E-H.

These predictions provide a theoretical explanation for previous empirical observations about the importance, relative to other traits, of development rate to ectotherm thermal fitness (*28, 29*) as well as its propensity to peak at higher temperatures, relative to other traits, in ectotherms adapting to warmer temperatures (*30, 31*). The fact that increasing the T_{pk}s of certain traits relative to others is predicted to increase population fitness is also important from

the perspective of constraints on evolution of thermal fitness. For example, when populations are confronted with long-term climatic warming (across generations), we expect the T_{pk}s of development rate and maximum fecundity to shift first, and set the upper limit on how fast the local population can respond to temperature change.

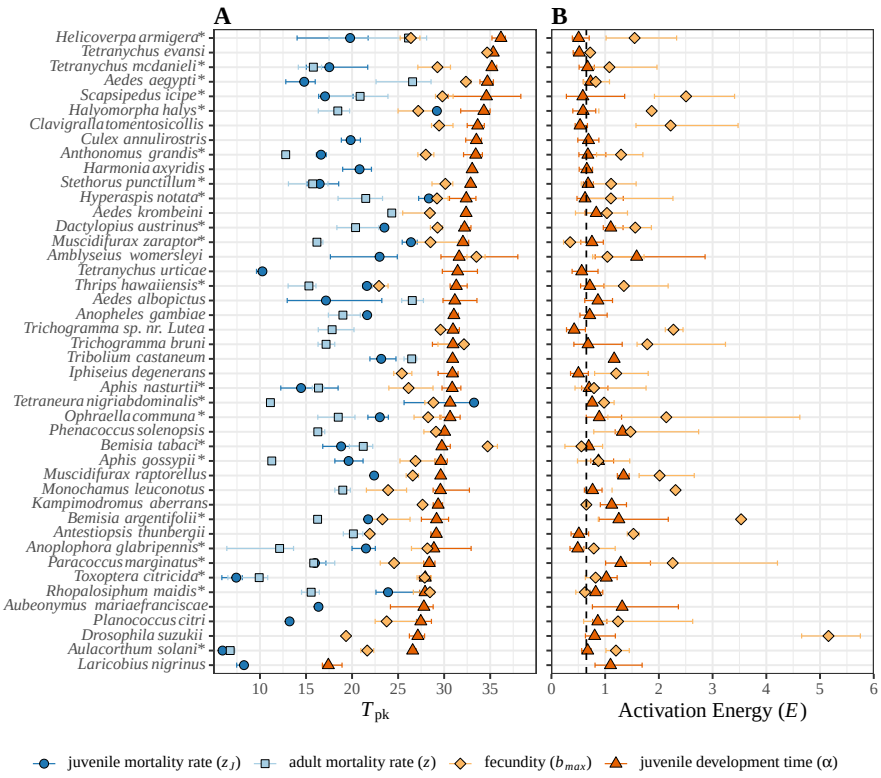

Figure 3: Empirical patterns in arthropod trait peak temperatures (T_{pk}s) (A) and thermal sensitivities (Es) (B). The bars around the T_{pk} estimates are 95% confidence intervals obtained by bootstrapping (residual resampling) the NLLS fits. Species for whom the full complement of trait data necessary for evaluating the r_m model (SM Eqn 2) are denoted with asterisks. Species that did not have data for α (n=10) or only had α (n=7) are included in SM Fig. 1.

To test the theoretical prediction that the trait TPCs underlying thermal fitness have evolved in a hierarchical way, we performed an extensive empirical data synthesis covering 61 diverse arthropod species (Fig. 3A, Materials and Methods). We first tested for the predicted existence of a hierarchical ordering of within-species trait T_{pk}s due to temperature-mediated life history optimization. We found that the empirical patterns are remarkably consistent with this prediction (Fig. 2). Development rate almost always exhibits a higher T_{pk} than peak fecundity, adult mortality rate, or juvenile mortality rate, and among the latter three, the ordering is typically as predicted. Furthermore, in the 22 species for which we were able to find data for all four of the traits, the ordering of T_{pk}s in 55% is exactly as predicted ($T_{pk}^{b_{max}} > T_{pk}^{z_J} > T_{pk}^{z}$), and in all

but three species, the T_{pk} of development rate is higher than that of all other traits. This result remains robust to phylogenetic correction (SM Section 2.8). Also, as expected from ecological metabolic theory (*9, 13, 22*), the thermal sensitivity parameter (E) of trait TPCs are relatively constrained across species (Fig. 3B).

Physiological mismatches reduce thermal fitness

We next focused our analysis on variation among the T_{pk}s of life history traits and the role of potential trade-offs between them in constraining the optimization of thermal fitness (thermal fitness). Our theory predicts that at a given temperature, the simultaneous maximisation of multiple trait T_{pk}s should increase thermal fitness exponentially (Fig. 4A). That is, thermal fitness is exponentially higher if the T_{pk}s of all traits increase in concert in a warmer environment. For example, if T_{pk} of development rate increases, the emergent thermal fitness will be higher if the T_{pk}s of all other traits increase with it, than if they do not. This result, along with our selection gradient analysis (Fig. 2), predicts that in arthropods, selection should favor not just a maximization of T_{pk}^{α} relative to the T_{pk}s of other traits, but also a minimization of differences in T_{pk}s among traits. We call these differences between T_{pk}s "physiological mismatches". However, while theoretically optimal, a concerted increase in trait T_{pk}s may not be possible because of metabolic constraints because given a fixed energy budget, energy can be allocated to, say, either maximize development rate or fecundity rate, but not both (*32, 33*).

Constrained thermal adaptation in contemporary populations

The analysis of our empirical data indicates that there are indeed substantial physiological mismatches in traits across diverse taxa, especially between traits at the two ends of the selection strength hierarchy (Fig. 3A). In particular, the four species with the highest T_{pk}s for development rate (*H. armigera*, *T. mcdanieli*, *A. aegypti*, and *S. icipe*) have as much as a $\sim$20°C mismatch with the T_{pk}s of juvenile mortality and adult mortality rates. This suggests that the maximisation of performance of multiple traits at the same temperature is somehow constrained. To test whether arthropod traits have nevertheless evolved to achieve maximal fitness within the constraints imposed by trade-offs, we overlaid the estimated thermal fitness from the data synthesis on to the theoretically-predicted optimal region. We found that real thermal fitness values of diverse arthropod taxa do indeed lie within our theoretically-predicted ranges (Fig. 4A). Furthermore, this thermal life history optimization operates under thermodynamic constraints as seen by a hotter-is-better pattern in thermal fitness (Fig. 4B). Also, as expected, thermal fitness and its hotter-is-better pattern is strongly predicted by the (mass-corrected) value of development rate at its T_{pk} (Fig. 4C; also see SM Section 2.2). We also find that as expected (and assumed by our theory) the underlying traits (and most crucially, α) too follow a hotter-is-better pattern (SM Section 2.1). Finally, that these empirical patterns across diverse taxa are the result of long-term thermal evolution are further supported by our phylogenetic analysis (SM Section 2.8) as well as information about the native thermal environments of these taxa (SM Section

2.3-2.4). The constraints imposed by trade-offs between traits' performances is not unexpected and are known to limit fitness optimization in other contexts (*34*). Our study provides evidence for such constraints on thermal adaptation in arthropods in a nuanced yet general manner.

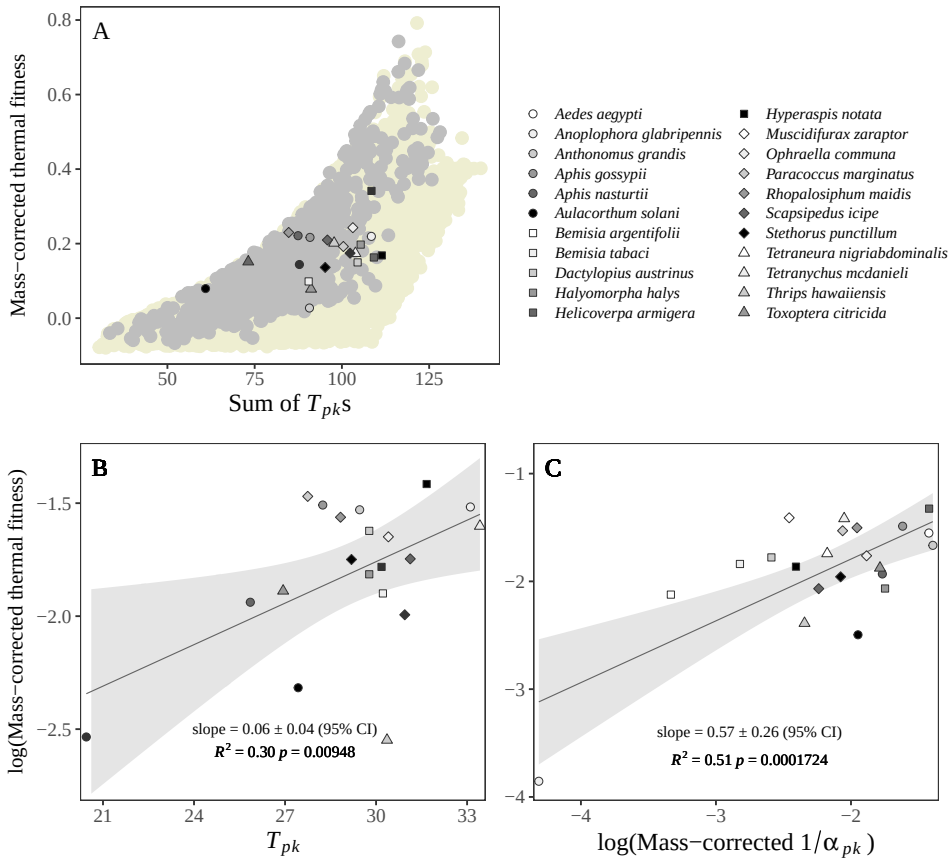

Figure 4: Effect of physiological mismatches on thermal fitness. A: Thermal fitness increases with the sum of trait T_{pk}s, which quantifies the simultaneous maximisation (optimization) of trait TPCs. The pale yellow dots represent simulated thermal fitness obtained by randomly varying T_{pk}s of all traits 5000 times by drawing them from a uniform distribution between of $10 - 35$°C (SM Materials and Methods) without constraining the ordering of the trait T_{pk}s. Among these, the subset of light grey dots satisfy the predicted hierarchy of trait selection strengths (are closer to an optimal strategy of $T_{pk}^{\alpha} > T_{pk}^{b_{max}} > T_{pk}^{z_J} > T_{pk}^{z}$) (Fig. 2). The thermal fitness values for 22 species (Fig. 3) with sufficient trait data are overlaid on these theoretically-predicted strategies. **B & C**: Thermal fitness increases with optimal temperature across a diverse group of arthropod taxa. **B:** The temperature dependence of mass-corrected optimal r_m ($r_{m,opt}/M^{-0.1}$) predicted by SM Eqn 2. **C:** Consistent with our theoretical prediction, mass-corrected optimal thermal fitness ($r_{m,opt}/M^{-0.1}$) increases linearly (in log-scale) with mass-corrected development rate T_{pk}s ($(1/\alpha_{pk})/M^{-0.27}$).

Conclusions

The relatively simple theoretical framework we have developed here can be used to mechanistically predict the temperature dependence of arthropod population fitness and adaptation potential or vulnerability. It requires data on the temperature-dependencies of a small set of key, commonly-measured life history traits, and in principle, should be applicable to any arthropod population with stage-structured life history. It can be used to leverage relatively measurable traits to predict thermal fitness and adaptive potential across arthropod taxa, addressing a long-standing need (*8, 11, 35*). The approach could guide conservation and risk assessment efforts by looking across species to identify those most at risk of extinction and those most likely to expand their distributions in the face of climatic shifts. Our study indicates that the differences in the environmental conditions experienced by juvenile and adult life stages of arthropods warrants greater consideration and may hold the key to general approaches for predicting and developing interventions to counteract the effects of warming on beneficial as well as harmful species.

References

1. Y. M. Bar-On, R. Phillips, R. Milo, The biomass distribution on Earth, *Proc. Natl. Acad. Sci. U. S. A.* **115**, 6506–6511 (2018).

2. D. L. Wagner, E. M. Grames, M. L. Forister, M. R. Berenbaum, D. Stopak, Insect decline in the Anthropocene: Death by a thousand cuts, *Proc. Natl. Acad. Sci. U. S. A.* **118**, 1-10 (2021).

3. R. Van Klink, *et al.*, Meta-analysis reveals declines in terrestrial but increases in freshwater insect abundances, *Science* **368**, 417–420 (2020).

4. M. S. Crossley, *et al.*, No net insect abundance and diversity declines across us long term ecological research sites, *Nat. Ecol. Evol* **4**, 1368–1376 (2020).

5. S. Marta, M. Brunetti, R. Manenti, A. Provenzale, G. F. Ficetola, Climate and land-use changes drive biodiversity turnover in arthropod assemblages over 150 years, *Nat. Ecol. Evol* **5**, 1291–1300 (2021).

6. J. E. Heath, J. L. Hanegan, P. J. Wilkin, M. S. Heath, Adaptation of the thermal responses of insects, *Integr. Comp. Biol.* **11**, 147–158 (1971).

7. A. Jensen, T. Alemu, T. Alemneh, C. Pertoldi, S. Bahrndorff, Thermal acclimation and adaptation across populations in a broadly distributed soil arthropod, *Funct. Ecol.* **33**, 833–845 (2019).

8. A. A. Hoffmann, C. M. Sgrò, Climate change and evolutionary adaptation, *Nature* **470**, 479–85 (2011).

9. A. I. Dell, S. Pawar, V. M. Savage, Systematic variation in the temperature dependence of physiological and ecological traits, *Proc. Natl. Acad. Sci. U. S. A.* **108**, 10591–10596 (2011).

10. M. Frazier, R. B. Huey, D. Berrigan, Thermodynamics constrains the evolution of insect population growth rates:"warmer is better", *Am. Nat.* **168**, 512–520 (2006).

11. M. J. Angilletta Jr, *Thermal adaptation: a theoretical and empirical synthesis* (Oxford University Press, 2009).

12. L. J. Cator, *et al.*, The role of vector trait variation in vector-borne disease dynamics, *Front. Ecol. Evol.* **8**, 189 (2020).

13. P. Amarasekare, V. Savage, A framework for elucidating the temperature dependence of fitness, *Am. Nat.* **179**, 178–91 (2012).

14. L. B. Jørgensen, M. Ørsted, H. Malte, T. Wang, J. Overgaard, Extreme escalation of heat failure rates in ectotherms with global warming, *Nature* pp. 1–6 (2022).

15. K. Duffy, T. C. Gouhier, A. R. Ganguly, Climate-mediated shifts in temperature fluctuations promote extinction risk, *Nat. Clim. Change* pp. 1–21 (2022).

16. H. Weaving, J. S. Terblanche, P. Pottier, S. English, Meta-analysis reveals weak but pervasive plasticity in insect thermal limits, *Nat. Commun.* **13**, 5292 (2022).

17. C. A. Deutsch, *et al.*, Impacts of climate warming on terrestrial ectotherms across latitude, *Proc. Natl. Acad. Sci. U. S. A* **105**, 6668–6672 (2008).

18. D. P. Brass, *et al.*, Phenotypic plasticity as a cause and consequence of population dynamics, *Ecol. Lett.* **24**, 2406–2417 (2021).

19. L. B. Buckley, J. G. Kingsolver, Evolution of thermal sensitivity in changing and variable climates, *Annu. Rev. Ecol. Evol. Syst.* **52**, 563–586 (2021).

20. J. G. Kingsolver, *et al.*, Complex life cycles and the responses of insects to climate change, *Integr. Comp. Biol.* **51**, 719–732 (2011).

21. J. G. Kingsolver, The well-temperatured biologist, *Am. Nat.* **174**, 755–768 (2009).

22. D.-G. Kontopoulos, *et al.*, Phytoplankton thermal responses adapt in the absence of hard thermodynamic constraints, *Evolution* **74**, 775–790 (2020).

23. B. J. Sinclair, C. M. Williams, J. S. Terblanche, Variation in thermal performance among insect populations, *Physiol. Biochem. Zool.* **85**, 594–606 (2012).

24. J. L. Maino, J. D. Kong, A. A. Hoffmann, M. G. Barton, M. R. Kearney, Mechanistic models for predicting insect responses to climate change, *Curr. Opin. Insect Sci.* **17**, 81–86 (2016).

25. M. J. Angilletta, R. B. Huey, M. R. Frazier, Thermodynamic effects on organismal performance: Is hotter better?, *Physiol. Biochem. Zool.* **83**, 197–206 (2010).

26. R. Schoolfield, P. Sharpe, C. Magnuson, Non-linear regression of biological temperature-dependent rate models based on absolute reaction-rate theory, *J. Theor. Biol.* **88**, 719–731 (1981).

27. D. A. Asbury, M. J. Angilletta, Thermodynamic effects on the evolution of performance curves, *Am. Nat.* **176**, E40–E49 (2010).

28. P. J. Huxley, K. A. Murray, S. Pawar, L. J. Cator, The effect of resource limitation on the temperature dependence of mosquito population fitness, *Proc. R. Soc. B* **288**, rspb.2020.3217 (2021).

29. P. J. Huxley, K. A. Murray, S. Pawar, L. J. Cator, Competition and resource depletion shape the thermal response of population fitness in *Aedes aegypti*, *Commun. Biol* **5**, 1–11 (2022).

30. R. B. Huey, D. Berrigan, Temperature, demography, and ectotherm fitness, *Am. Nat.* **158**, 204–210 (2001).

31. D. L. Trudgill, Why do tropical poikilothermic organisms tend to have higher threshold temperatures for development than temperate ones?, *Funct. Ecol.* **9**, 136–137 (1995).

32. N. Tüzün, R. Stoks, A fast pace-of-life is traded off against a high thermal performance, *Proc. R. Soc. B* (2022).

33. L. C. Birch, The intrinsic rate of natural increase of an insect population, *J. Anim. Ecol.* **17**, 15 (1948).

34. S. C. Stearns, Trade-offs in life-history evolution, *Funct. Ecol.* **3**, 259–268 (1989).

35. H. O. Pörtner, *et al.*, Trade-offs in thermal adaptation: the need for a molecular to ecological integration, *Physiol. Biochem. Zool.* **79**, 295–313 (2006).

Acknowledgements

Author contributions: SP and LC conceived the study. SP developed the theory with support from TS and LJ. PH collated and analysed the data with support from AC, MN, and MS. DK performed the phylogenetic analyses. All authors contributed to writing and revising the manuscript.

Data and code availability

All data and code for reproducing the study's analyses can be found at `https://github.com/PawarLab/TraitMismatchPaper-main.git`. Our global dataset on arthropods is also available as an Auxiliary Supplementary file (Appendix 1).

Supplementary Materials for

Variation in temperature of peak trait performance will constrain adaptation of arthropod populations to climatic warming

Samraat Pawar *et al.*
Corresponding authors: Samraat Pawar, s.pawar@imperial.ac.uk;
Paul J. Huxley, phuxley@vt.edu; Lauren Cator, l.cator@imperial.ac.uk

January 17, 2023

Contents

1 Materials and Methods **1**
1.1 The model for temperature-dependent maximal population growth rate . . . 1
1.2 Trait sensitivity analysis . . . 3
1.3 Quantifying trait-specific selection gradients . . . 3
1.4 Quantifying effects of physiological mismatches . . . 3
1.5 Data synthesis . . . 4
1.6 Phylogenetic analyses . . . 5
1.6.1 Phylogeny construction . . . 5
1.6.2 Investigation of the macroevolutionary patterns of T_{pk}s . . . 5

2 Supplementary Results **7**
2.1 Trait-level "hotter-is-better" patterns . . . 7
2.2 Correlation of thermal fitness with peak trait performance . . . 8
2.3 Evidence of trait-level thermal adaptation . . . 9
2.4 Distributions of trait-level thermal sensitivities . . . 12
2.5 Trait-level thermal performance curves . . . 13
2.6 Species-level temperature dependencies of r_m . . . 17
2.7 Sensitivity of the results to the parameterisation of fecundity loss rate (κ) . . . 18
2.7.1 Effect on the trait sensitivity results . . . 19
2.7.2 The selection gradients revisited . . . 19
2.8 Macroevolutionary patterns and phylogenetic constraints . . . 20

1 Materials and Methods

1.1 The model for temperature-dependent maximal population growth rate

Our model for r_m is based on the Euler-Lotka equation (1; 2; 3):

$$\int_{\alpha}^{\infty} e^{-r_m x} l_x b_x dx = 1, \tag{1}$$

where α is the age at first reproduction (the time needed for development from egg to adult, or the juvenile to adult development time); l_x is age-specific survivorship (proportion of individuals that survive from birth to age x); and b_x the age-specific fecundity (number of offspring produced by an individual of age x). This equation gives the expected reproductive success of a newborn individual in a population growing at a rate r_m, under the assumption that the population has reached a stable age distribution (i.e., the proportion of individuals in adult and juvenile life stages is constant). Using the simplest feasible mortality and fecundity models (for l_x and b_x respectively), we previously derived an approximation appropriate for the range of growth rates typically seen across arthropods (4) (Table 1):

$$r_m \approx \frac{(\kappa + z)\left(\log\left(\frac{b_{max}}{\kappa+z}\right) - \alpha z_J\right)}{\alpha(\kappa + z) + 1}. \tag{2}$$

Table 1: Definitions of model parameters.

Parameter	Units	Description
r_m	day^{-1}	Maximal population growth rate
α	days	Egg to adult development time
b_{max}	eggs $\times$ (female $\times$ day)$^{-1}$	Maximum fecundity rate
κ	day^{-1}	Fecundity loss rate
z	day^{-1}	Adult mortality rate
z_J	day^{-1}	Mortality rate averaged across juvenile stages
B	measurement unit of trait	Trait value at a given temperature
B_0	measurement unit of trait	Normalisation constant for trait value at T_{ref}
T_{pk}	°C or K	Temperature at which trait performance peaks
B_{pk}	Measurement unit of trait	Trait performance achieved at T_{pk}
T_{opt}	°C or K	Temperature at which r_m peaks
r_{opt}	day^{-1}	r_m achieved at T_{opt}
E	eV	Activation energy
E_D	eV	Deactivation energy
k	eV K^{-1}	Universal Boltzmann constant ($8.617 \cdot 10^{-5}$)

Substituting models of the thermal performance curves (TPCs) of the five life history traits (Section 2.5) into Eqn 2 gives the temperature-dependence of r_m. We model these traits TPCs using the modified Sharpe-Schoolfield equation (5; 6) or its inverse (Main text Fig. 1):

$$B = B_0 \frac{(E_D - E)e^{\frac{-E}{k}\left(\frac{1}{T} - \frac{1}{T_{ref}}\right)}}{E_D - E + Ee^{\frac{E_D}{k}\left(\frac{1}{T_{pk}} - \frac{1}{T}\right)}}. \tag{3}$$

Here B is the value of the metabolic trait at a given temperature (T, in degrees K); B_0 is a normalisation constant representing the value of the trait at some reference temperature (T_{ref}); E is the apparent activation energy (initial thermal sensitivity), which determines how fast the curve rises up as the temperature approaches the peak temperature, T_{pk}; and E_D is the deactivation energy, which determines how fast the trait declines after the peak. The parameter k is the universal Boltzmann constant ($8.617 \cdot 10^{-5}$ eV K^{-1}). The constant B_0 also includes the effect of body size, and therefore the effect of stage-specific size differences, which we do not explicitly consider here theoretically, but will consider in the data we analyze (below; also see Discussion). Equation (3) has been used as a model for thermal performance of traits in numerous previous studies on arthropod population biology because it accurately captures the temperature dependence of a wide range of metabolically constrained life history traits (e.g., 7; 8; 9). For

mortality rates (z and z_j), we use the inverse of equation (3) because the thermal response of mortality rate tends to be U-shaped (10; 11; 12), and is well-fitted by it (8; 13). Using a different unimodal function instead of the Sharpe-Schoolfield equation will not qualitatively change our results provided that it can encode a "hotter-is-better" constraint (14). Substituting the trait TPCs into Equation (2) yields the TPC of r_m, from which we numerically calculate the T_{opt} (temperature at which the optimum of population growth occurs) and r_{opt} (the value of r_m at T_{opt}). Note that we refer to the temperature of peak r_m as T_{opt} rather than T_{pk} as we do for traits, because the T_{pk}s of those traits do not necessarily correspond to the thermal optimum of population fitness (optimal thermal fitness).

1.2 Trait sensitivity analysis

To determine how much influence individual traits' TPCs have on r_m's temperature-dependence, using the chain rule, we can write (10; 4):

$$\frac{\mathrm{d}r_m}{\mathrm{d}T} = \frac{\partial r_m}{\partial b_{max}}\frac{\mathrm{d}b_{max}}{\mathrm{d}T} + \frac{\partial r_m}{\partial \alpha}\frac{\mathrm{d}\alpha}{\mathrm{d}T} + \frac{\partial r_m}{\partial z}\frac{\mathrm{d}z}{\mathrm{d}T} + \frac{\partial r_m}{\partial z_J}\frac{\mathrm{d}z_J}{\mathrm{d}T} + \frac{\partial r_m}{\partial \kappa}\frac{\mathrm{d}\kappa}{\mathrm{d}T} \tag{4}$$

Each summed term in the right hand side of this equation quantifies the relative contribution of the TPC of a parameter to the temperature dependence of r_m (Main text Fig. 1C). The trait TPCs for this calculation were parameterized as described above with and identical $T_{pk} = 25°\mathrm{C}$ across all traits. Here again, the choice of the TPC parameters, as long as all the B_0s are in their appropriate scale, do not change the results of this trait-sensitivity analysis qualitatively.

1.3 Quantifying trait-specific selection gradients

In order to quantify the impact of changes in T_{pk}s of different traits on r_m's temperature-dependence (i.e., the thermal selection gradient on each trait), we calculated the shift in optimal maximum population growth rate (r_{opt}), i.e., the value of r_m at T_{opt} with a unit change in each trait's T_{pk}. For this, re-evaluated Eqn 2 by varying each trait's T_{pk} in turn while holding all other trait TPCs constant at 25°C (approximately the median of all the values observed in the data; Main Text Fig. 3), over a temperature range of 0–35°C (Main text Fig. 2). That is, we allowed T_{pk} of each focal trait, in turn, to vary from -10 to +15 °C relative to $T_{pk} = 25°\mathrm{C}$, keeping all other trait TPCs (including their T_pks) fixed. This ensured that the T_{pk}s of any given trait varied between 15°C – 40°C, which is approximately the range seen in the empirical data (see below; Main text Fig. 3). We denote the difference of the focal trait's T_{pk} from those of all others as ΔT^{α}_{pk}, ΔT^{z}_{pk}, etc. The strength of the directional selection gradient for each trait was calculated as the second derivative $\frac{\partial^2 r_{opt}}{\partial {T^{\theta}_{pk}}^2}$ (where θ is one of the four traits) (15; 16; 17; 18). The minimum of this quantity pinpoints the temperature at which that selection gradient starts to asymptote as serves as a prediction of the ordering of trait T_{pk}s that optimises thermal fitness (Main text Fig. 2). This method ignores trade-offs or covariances between traits, which would change the shape of the selection gradients (e.g., making them unimodal instead of asymptotic; see discussion in Main text, as well as the results of our phylogenetic analyses (below)).

1.4 Quantifying effects of physiological mismatches

Given that a higher $T_{pk,\alpha}$ increases fitness, and that all trait-specific selection gradients are monotonically increasing, closer the T_{pk}s of the other traits are to $T_{pk,\alpha}$, the higher the $r_{m,opt}$. We term the distance between any trait's T_{pk} and $T_{pk,\alpha}$ a "physiological mismatch". To quantify the effect of the overall level of physiological mismatch across all pairwise combinations of $T_{pk,\alpha}$ and each of the other three traits, we used the sum of all T_{pk}s as a mismatch measure, which is a consistent measure because it increases monotonically with a decrease in mismatch. Then to calculate the effects of this overall physiological mismatch on thermal fitness, we quantified how r_{opt} changes with different potential life history strategies

(in terms or ordering of the T_{pk}s) it by randomly permuting their order. For this, all other TPC parameters were kept fixed (see next).

TPC parameterisations

For the numerical calculation of r_m's temperature-dependence, trait sensitivity, selection gradient analyses and physiological mismatch analyses (above), we parameterized the traits' TPC equations as follows. Firstly, because our theory focuses on the relative differences between the T_{pk}s of traits, the exact values of E and E_D do not matter as long as they lie within empirically-reasonable values, so we fixed them across all traits to be $E = 0.6$ and $E_D = 4$. These are approximately the median values found in our empirical data (Main text Fig. 3, SM Fig. 6). Varying these within the range seen in our empirical data do not change our results qualitatively. The parameter values for B_0 were varied with type of trait, fixing them to be (approximately, rounded) the median values observed in our empirical data at a T_{ref} of 10°C: $B_{0,\alpha} = 25$, $B_{0,b_{max}} = 1$, $B_{0,z} = 0.03$, and $B_{0,z_J} = 0.05$ (SM Fig.7-10). In the absence of data on the rate of loss of fertility (κ) or its TPC, we evaluated the model's predictions for a range of values of this parameter (SM section 2.7). While the values for all these parameters in the real data vary considerably around their respective medians, these specific ones used throughout the manuscript's theory figures suffice to generate qualitatively-robust theoretical predictions.

1.5 Data synthesis

We performed an extensive literature search to collate existing data on the TPCs of individual traits across arthropod taxa. We searched for publications up to July 2022 using Google Scholar's advanced search, using Boolean operators (e.g., life history AND pest OR vector AND temper*), without language restrictions. Additional searches were also made by including species' names in the search string to improve the detection of publications on under-represented groups. For some species, multiple data sets were available so we only included the study that provided the most complete data (i.e., the highest number of traits measured). Raw data and references are available in Appendix 1. We excluded all field studies, and also lab studies where traits had been measured over narrow (< 10°C) temperature ranges (that prevented reliable TPC model fitting; below). We also excluded species from our analysis of physiological mismatches if TPC data for at least two traits were not available for them. Values of relevant traits across temperatures at were extracted from the text or tables, or were read from the figures using WebPlotDigitizer (19). All data were converted to consistent measurement units. If juvenile mortality rate (z_J, individual^{-1} day^{-1}) was not provided (most of the original studies), we divided juvenile survival proportion by development time. Similarly, if adult mortality rate (z) was not directly reported, we calculated it as the reciprocal of (typically, female) longevity (1/days). When fecundity rate was not directly reported we divided lifetime reproductive output by longevity to obtain fecundity rate (b_{max}; eggs / (individual $\times$ day)$^{-1}$).

Finally, each species- and trait-specific thermal response dataset was fitted to the appropriate TPC equation (Eqn. (3) or its inverse; Fig.1A & B) using NLLS using the `rTPC` pipeline (20; 21). Bootstrapping (residual resampling) was used to calculate 95% prediction bounds for each TPC, which also yielded the confidence intervals around each T_{pk} and peak trait value (B_{pk}) estimate. These trait value estimates were body mass-corrected to adjust for how the temperature-dependence of r_m emerges from the temperature-dependencies of its underlying traits, which, in turn, are dependent on the relationships between body size and metabolic rate in individual organisms (2). If fresh mass (mg, M in Main text Fig.4 & SM Figs.1&2) for a particular species was not provided in the original study, we used mass estimates from other studies on that or a closely related species.

1.6 Phylogenetic analyses

1.6.1 Phylogeny construction

To examine the macroevolutionary patterns of the T_{pk}s of the four main traits of this study (α, b_{max}, z_J, and z), we first extracted the phylogenetic topology of all the species in our dataset from the Open Tree of Life (22) (OTL; v.13.4) using the `rotl` R package (23) (v.3.0.12). Given that the OTL topology (Fig. 13A) included a few polytomies, we also collected publicly available nucleotide sequences (where available) of: i) the 5' region of the cytochrome c oxidase subunit I gene (COI-5P); ii) the small subunit rRNA gene (SSU); and iii) the large subunit rRNA gene (LSU). COI-5P sequences were obtained from the Barcode of Life Data System database (24), whereas SSU and LSU sequences were extracted from the SILVA database (25) (Table 2).

Next we aligned the sequences with MAFFT (26) (v.7.490) using the G-INS-i algorithm for COI-5P sequences, and the X-INS-i algorithm for SSU and LSU sequences. We specifically chose the latter algorithm for the two rRNA genes as it can take the secondary structure of RNA into consideration while estimating the alignment (27). We then removed phylogenetically uninformative sites using the Noisy tool (28), and merged the alignments of the three genes into a single concatenated alignment. For each gene, we identified the optimal model of nucleotide substitution with ModelTest-NG (29; 30) (v.0.2.0), according to the small sample size-corrected Akaike Information criterion (31).

For phylogenetic topology inference based on the concatenated alignment, we employed the RAxML-NG tool (32) (v.1.1.0). We constrained the topology search based on the OTL tree, which allowed us to incorporate further phylogenetic information from previously published studies. Nevertheless, because we could not obtain molecular sequences for all species (SM Table 2), some of the polytomies of the OTL tree could not be objectively resolved. To account for this uncertainty in downstream analyses, we performed 100 topology searches, each of which started from 100 random and 100 maximum parsimony trees. This process yielded a set of 100 trees, in which 21 alternative topologies were represented (SM Fig. 13B).

To time-calibrate each of the 100 trees, we first queried the Timetree database (33) to obtain reliable age information (based on at least five studies) for as many nodes as possible. We then applied the "congruification" approach (34) implemented in the `geiger` R package (35) (v.2.0.10). In other words, we transferred known node ages (and their uncertainty intervals) from the reference phylogeny (TimeTree) to each of the 100 target phylogenies. This information was then used by the treePL tool (36) to estimate ages for all tree nodes based on penalized likelihood. SM Fig. 13B shows the the final set of the 100 alternative time-calibrated trees.

1.6.2 Investigation of the macroevolutionary patterns of T_{pk}s

To quantitatively characterise the evolution of the T_{pk}s of the four traits in this study, we fitted a Bayesian phylogenetic multi-response regression model with the `MCMCglmm` R package (37) (v.2.33). In particular, this model had all four T_{pk}s as separate response variables and one intercept per response. This allowed us to simultaneously estimate both the variances and covariances among the four T_{pk}s and, through this, to detect any systematic correlations. Furthermore, we specified a phylogenetic random effect on the intercepts by integrating the phylogenetic variance-covariance matrix into the model. By doing so, we partitioned the variance-covariance matrix of T_{pk}s into a phylogenetically heritable component and a residual component. The latter would reflect phylogenetically independent sources of variation in T_{pk} values (e.g., plasticity, experimental noise).

Given that we had information on the uncertainty of each T_{pk} estimate from bootstrapping, we directly incorporated this into the model. Missing T_{pk} values for one or more traits per species were modelled as "Missing At Random" (38; 39). This approach (not to be confused with "Missing Completely At Random") allows missing values in a response variable to be estimated (with some degree of uncertainty) from other covarying variables and from the phylogeny, provided that missingness is not systematically driven by a variable that is not included in the model (e.g., body size, habitat). Lastly, we specified uninformative

priors, namely the default normal prior for the fixed effects, a Cauchy prior for the random effects covariance matrix, and an inverse Gamma prior for the residual covariance matrix.

We fitted this model 100 times, each time with a different phylogenetic tree from our set, and with three independent chains per tree. We set the chain length to two hundred million generations and recorded posterior samples every five thousand generations, except for the first 10% of each chain (i.e., twenty million generations) which we discarded as burn-in. We then verified that the three chains per tree had statistically indistinguishable posterior distributions and had sufficiently explored the parameter space. For these, we ensured that the potential scale reduction factor value of each parameter was smaller than 1.1, and that its effective sample size was at least equal to 1,000.

Finally, we combined the posterior samples from the three chains of all 100 runs. From these, we first extracted the intercept and the phylogenetically heritable variance of each T_{pk}. The former represents the across-species mean whereas the latter corresponds to the evolutionary rate per million years. We additionally calculated the pairwise correlations between T_{pk}s and their phylogenetic heritabilities, that is, the ratio of the phylogenetically heritable variance to the sum of phylogenetically heritable and residual variances. We summarised these parameters by calculating the median value and the 95% Highest Posterior Density interval.

2 Supplementary Results

2.1 Trait-level "hotter-is-better" patterns

Across diverse levels of biological organisation, many biological rates (e.g., development, population growth) are expected to scale to the negative quarter-power with mass-specific metabolic rate ($M^{-0.25}$) but such scaling may not exist in arthropods (40). Therefore, prior to testing for trait-level "hotter-is-better" patterns, we fitted OLS models in log-log scale to the B_{pk} estimates (Main text Fig.4 and SM Figs.1&2) and the body mass (wet mass, mg) data for each species (Appendix 1). We also size-corrected optimal thermal fitness ($r_{m,opt}$) to account for size scaling in underlying traits (Main text Fig.4 and SM Fig.2).

Our theory assumes that a "hotter-is-better" pattern exists in the underlying traits. In particular, given its dominant effect, α should definitely exhibit this pattern. While data on this within-species are not currently available, we tested this assumption with data across species (Main Text Fig.4B; Fig. 1). We observe a significant "hotter-is-better" pattern for development time (α; Main text Fig. 4B) and maximum fecundity (b_{max}) (Fig. 1A and D), whereas the slopes for z_J and z are non significantly positive and negative, respectively. *Anoplophora glabripennis* was excluded from this analysis because it's r_{opt} was extremely low (r_{opt}=0.01). With this species included, the slope for seen in main text Fig. 4C becomes 0.09 ± 0.08 (95% CI), R^2=0.21 and p=0.03.

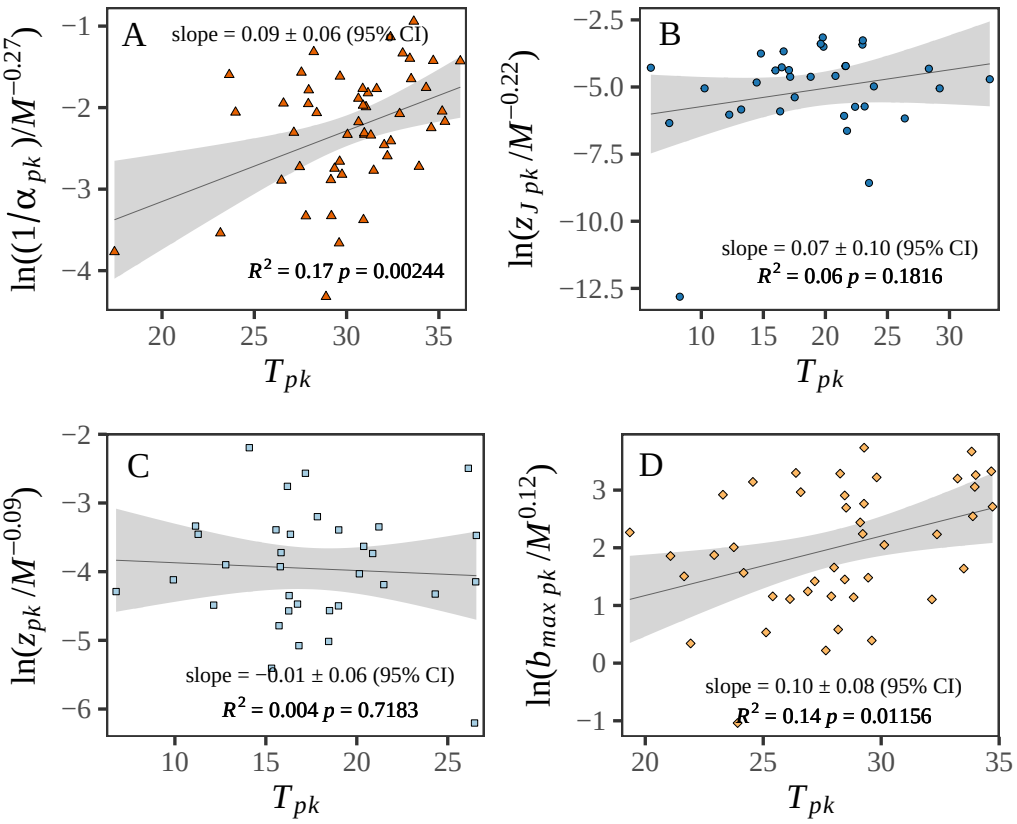

Figure 1: Test of the "hotter-is-better" pattern across arthropod taxa.The "hotter-is-better" pattern is significant in the body size-corrected (wet mass, mg) $1/\alpha$ (A) and z_J (B) data, but at best weak for b_{max} (D) and z (C), suggesting relatively greater biochemical adaptation to overcome thermodynamic constraints in these two traits (6; 41), insufficient data (note the narrow range of temperatures on x-axis for b_{max} in particular) (42), or both. The lines are OLS regression (with 95% prediction bounds) fitted to log-transformed B_{pk}s of the trait plotted against the respective T_{pk}s.

2.2 Correlation of thermal fitness with peak trait performance

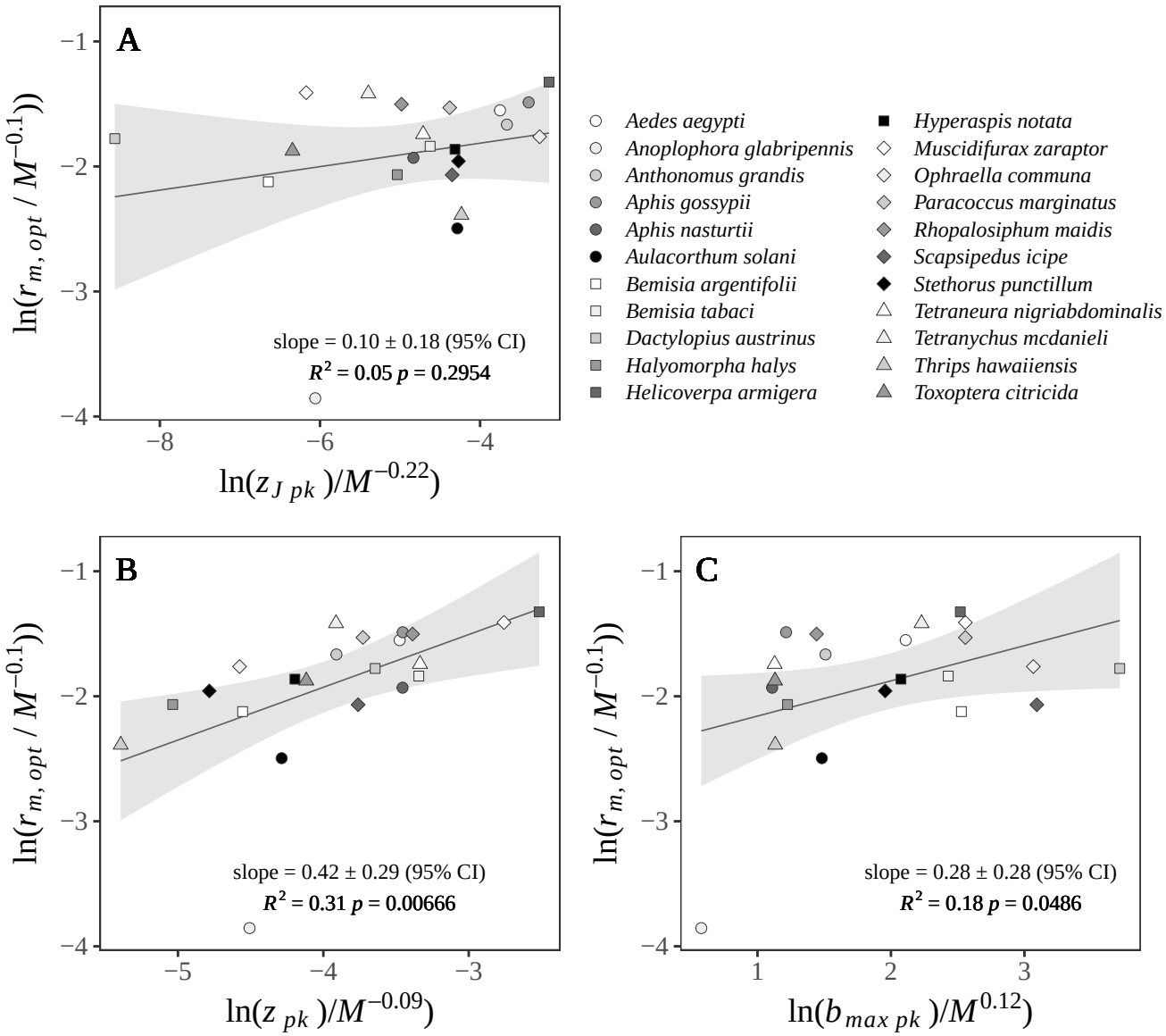

Figure 2: Relationship between $r_{m,opt}$ and peak A) juvenile mortality rate, B) adult mortality rate and C) fecundity rate. The lines are OLS regression (with 95% prediction bounds) fitted to log-transformed mass-corrected $r_{m,opt}$ plotted against the respective log-transformed mass-corrected trait T_{pk}s.

2.3 Evidence of trait-level thermal adaptation

To test for trait-level thermal adaptation, we first analysed the relationships between trait T_{pk}s and latitudes (i.e., the geographical locations where each experimental species originated from). All traits' T_{pk}s declined with increasing latitude, which suggests that species, albeit weakly, are adapted to their local environments (SM Fig. 3). because environmental variables other than temperature too vary with latitude we then also analysed the relationship between traits' T_{pk}s and rearing temperatures (i.e., the species' laboratory rearing temperatures; SM Fig.4), and rearing temperatures and latitudes (SM Fig.5). Traits' T_{pk}s increased significantly with rearing temperatures (SM Fig.4) and decreased significantly as latitudes increased. These results suggest that species originating from warmer climates were reared under warmer temperatures in the lab. Together, these results indicate the existence of significant existing trait-level thermal adaption amongst the species used in the present study.

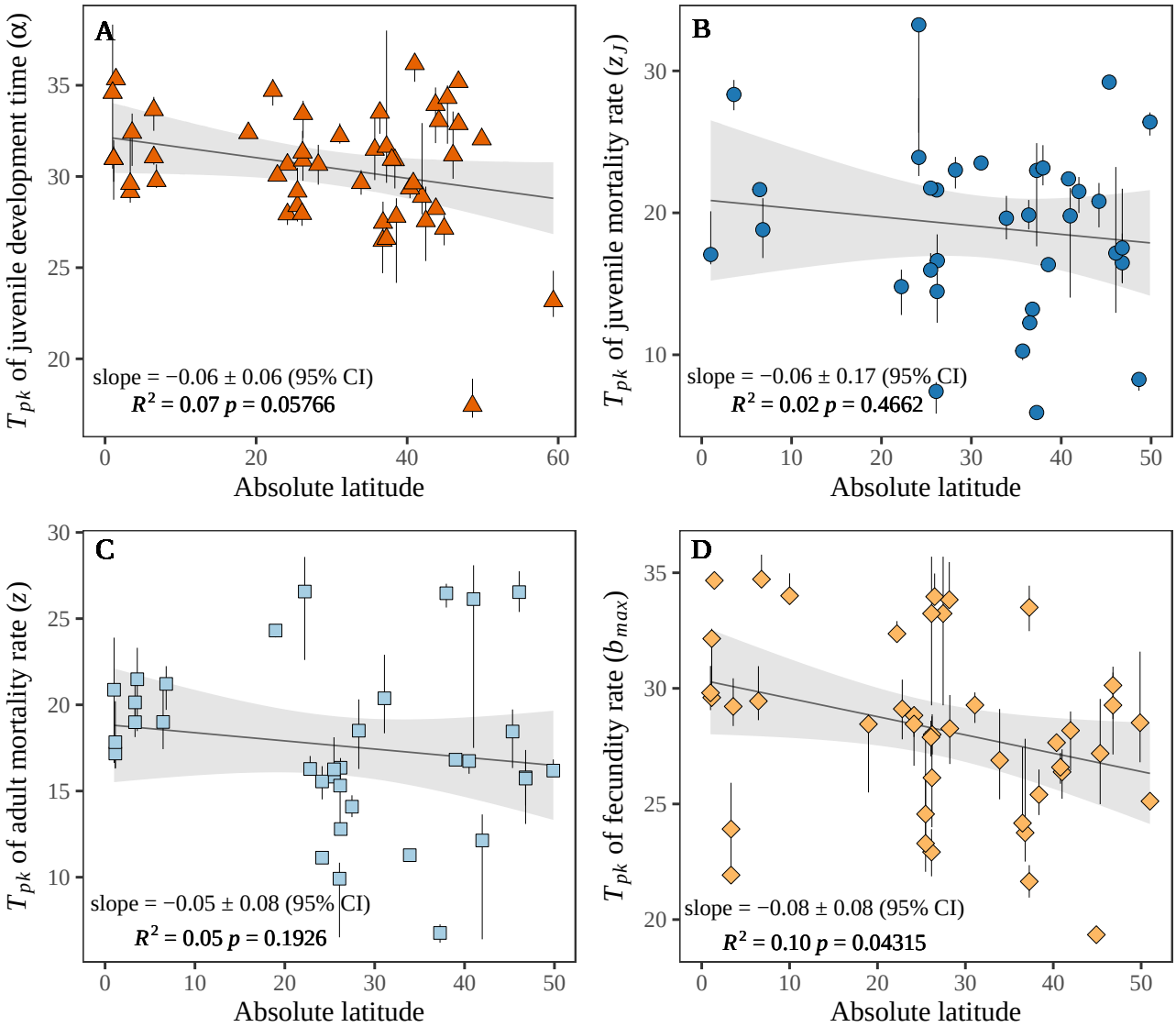

Figure 3: Relationship between latitude and T_{pk}s of A) juvenile development time, B) juvenile mortality rate, C) adult mortality rate and D) fecundity rate

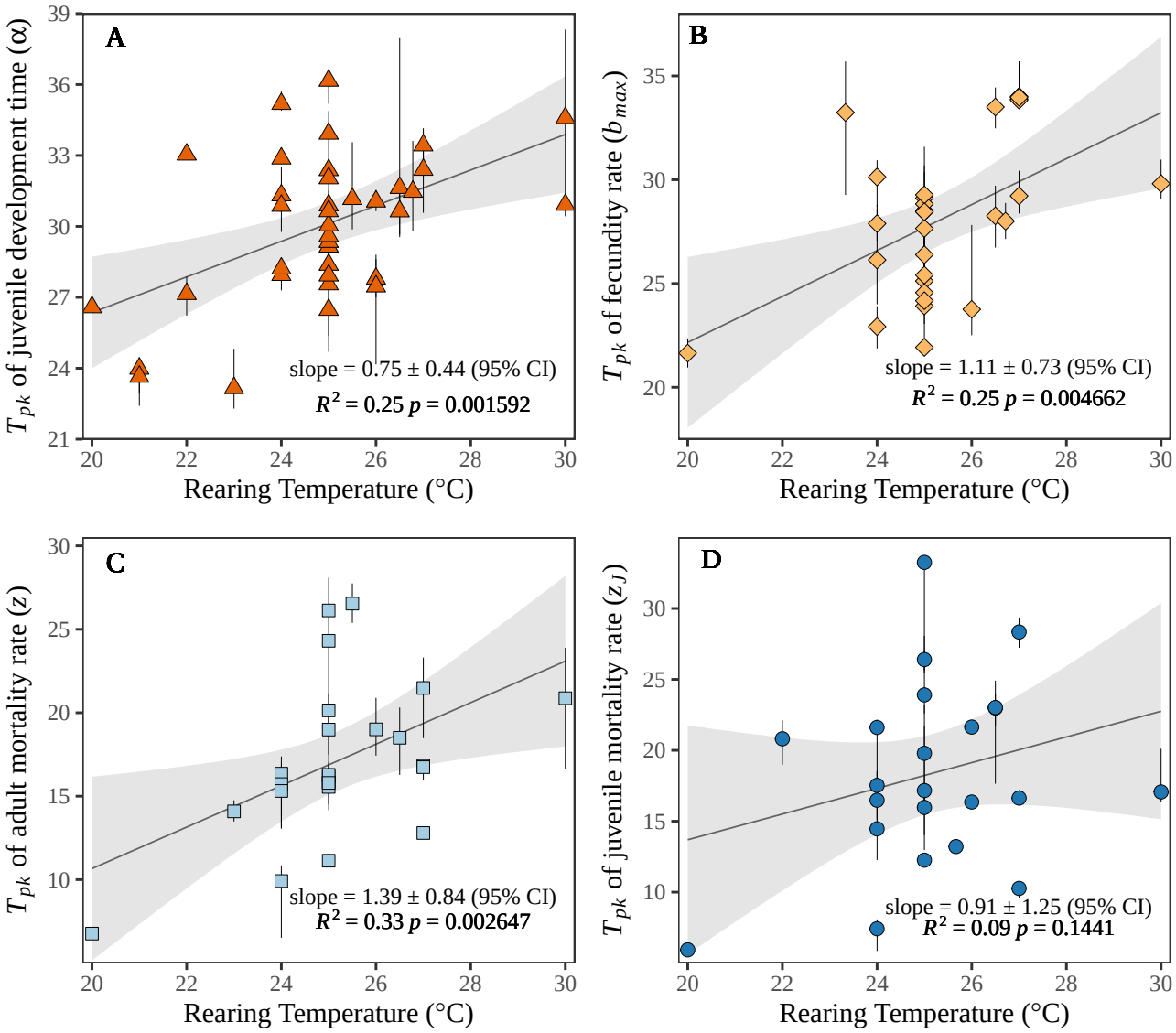

Figure 4: Relationship between rearing temperature and T_{pk}s of A) juvenile development time, B) juvenile mortality rate, C) adult mortality rate and D) fecundity rate

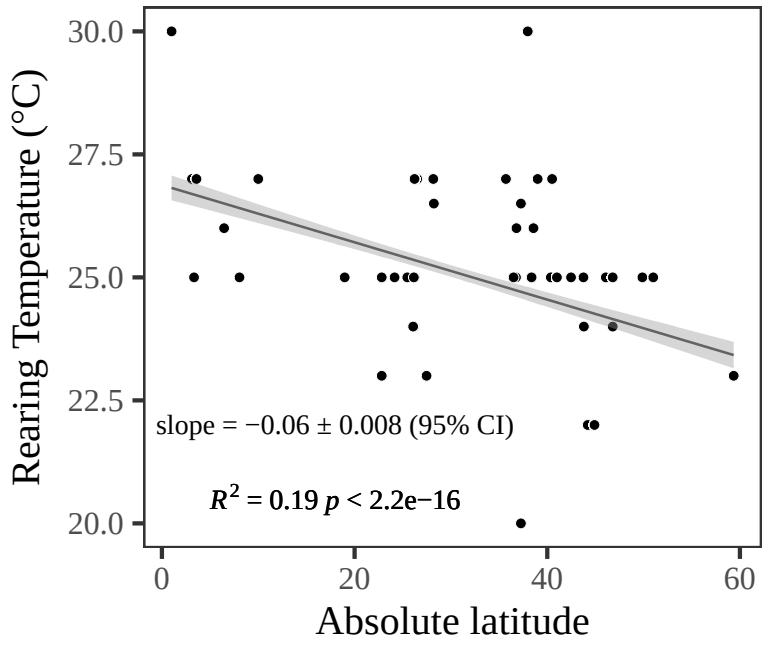

Figure 5: Relationship between rearing temperature and absolute latitude

2.4 Distributions of trait-level thermal sensitivities

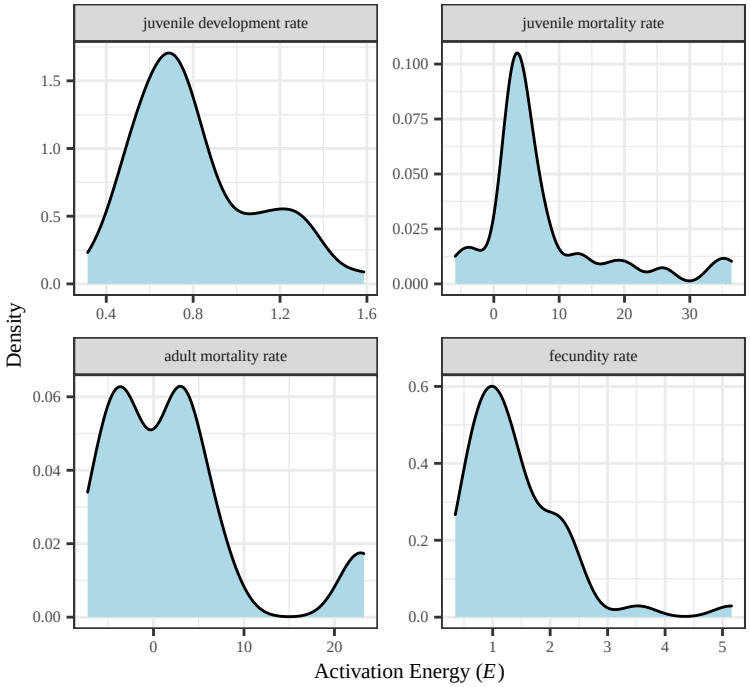

Figure 6: Distribution of estimated activation energy values for all fitted traits and species.

2.5 Trait-level thermal performance curves

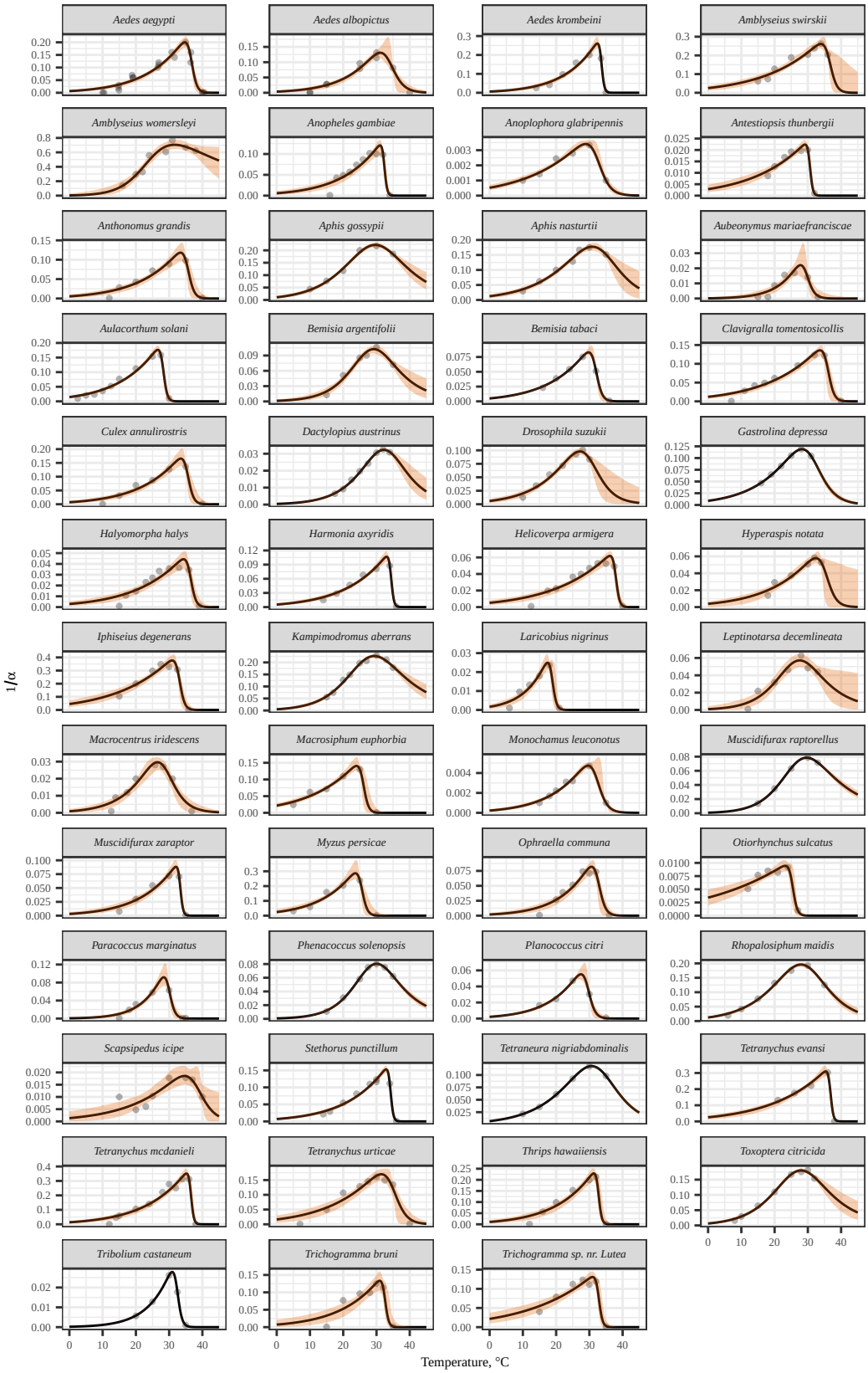

Figure 7: Thermal Performance Curve fits for all species: Development Rate

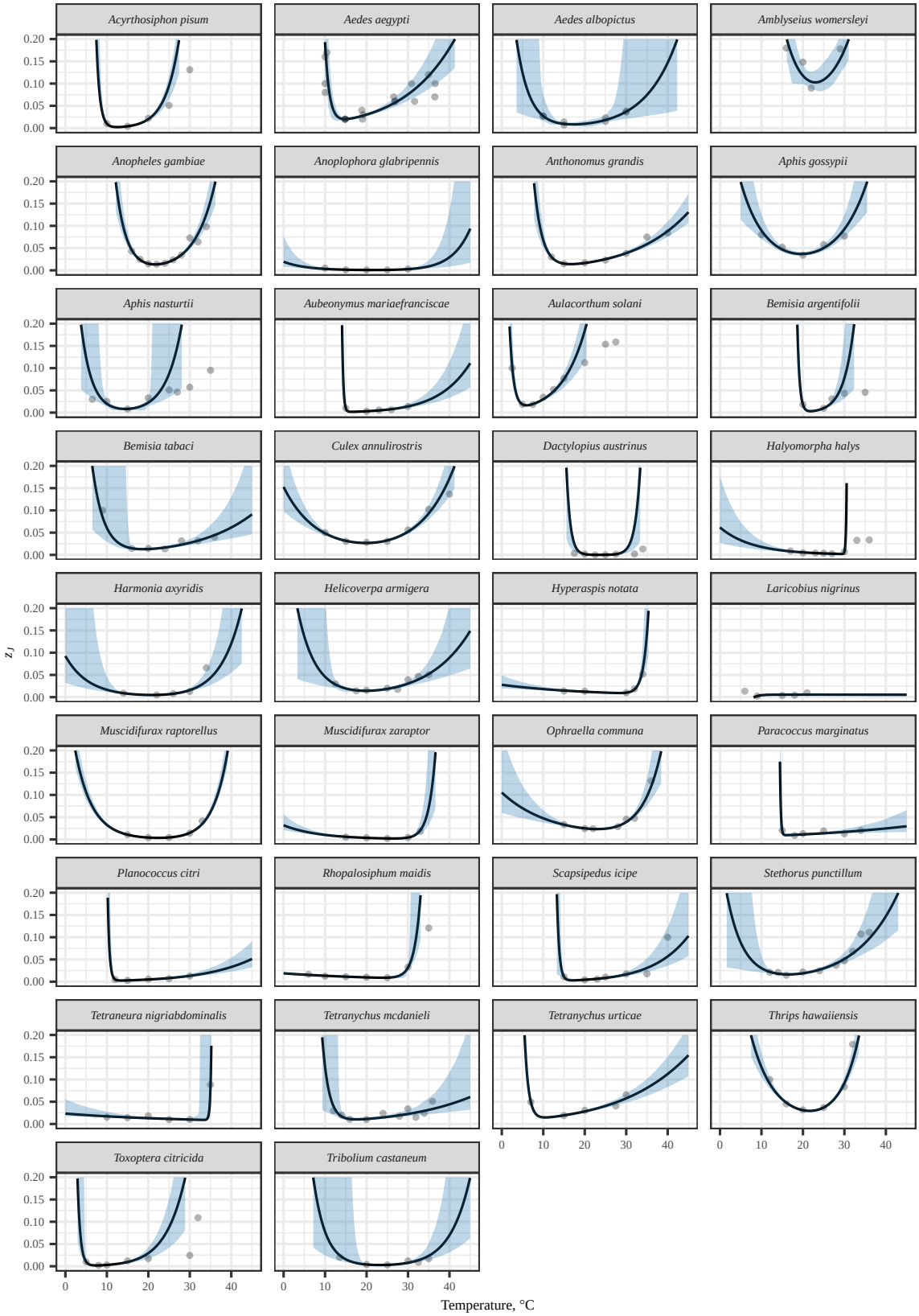

Figure 8: Thermal Performance Curve fits for all species: Juvenile Mortality

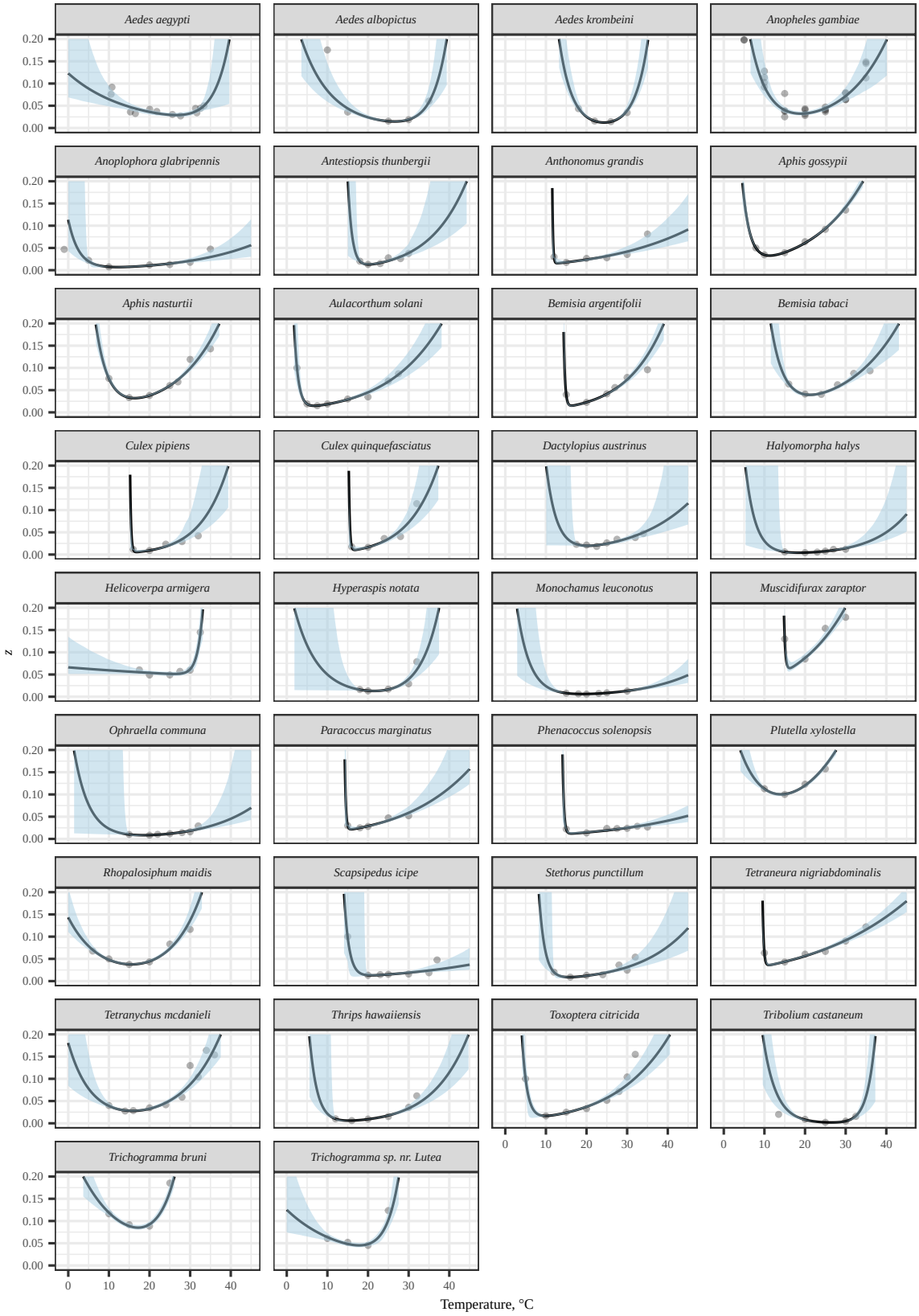

Figure 9: Thermal Performance Curve fits for all species: Adult Mortality

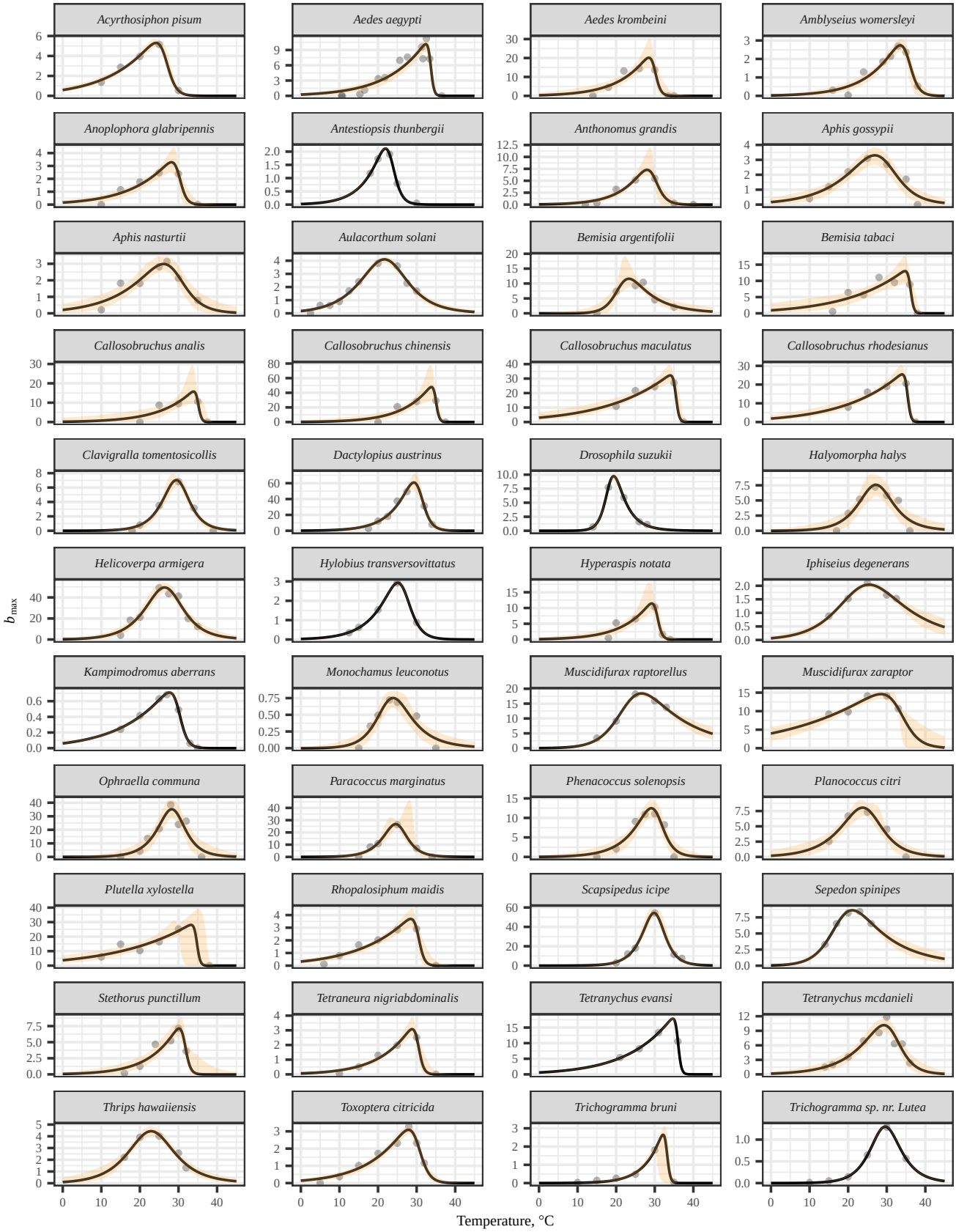

Figure 10: Thermal Performance Curve fits for all species: Fecundity

2.6 Species-level temperature dependencies of r_m

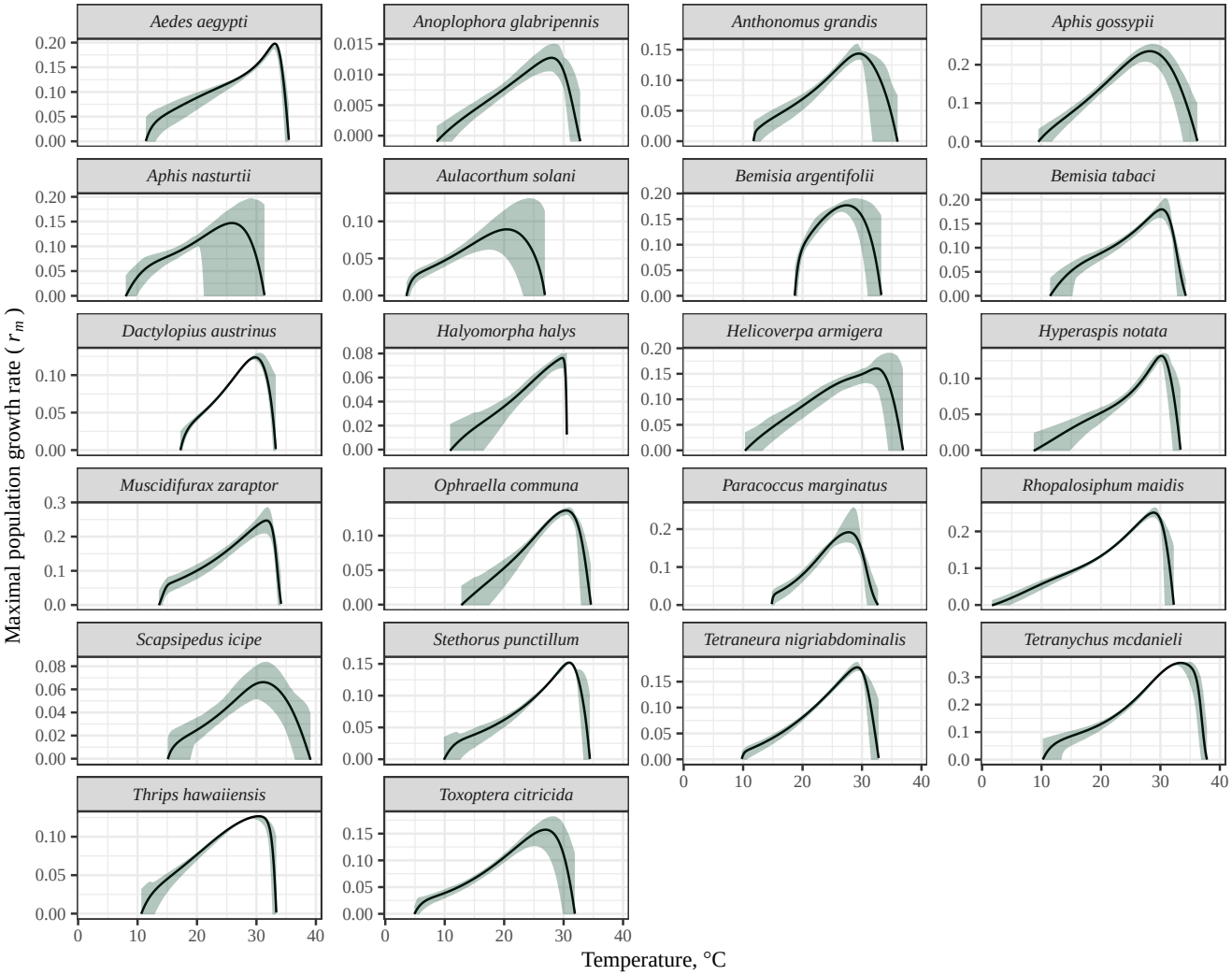

Figure 11: Thermal Performance Curve fits for all species: r_m

2.7 Sensitivity of the results to the parameterisation of fecundity loss rate (κ)

Fecundity typically declines over time, which can have significant impacts on the lifetime reproduction of individuals and therefore fitness. The rate at which fecundity declines with age (κ) may be temperature-dependent, but there appears to be practically no existing data on this for arthropods. Therefore, here we quantify the sensitivity of our theoretical predictions to changes in parameterisation of baseline fecundity loss rate (the normalisation constant, κ_0). Specifically, we re-evaluate our trait sensitivity analyses, as well as our calculation of selection gradient by varying κ_0 across two extreme values, around the value we have used to generate the main results (0.1). Figure 12 shows how changing κ_0 affects the shape of the fecundity curve at any given temperature.

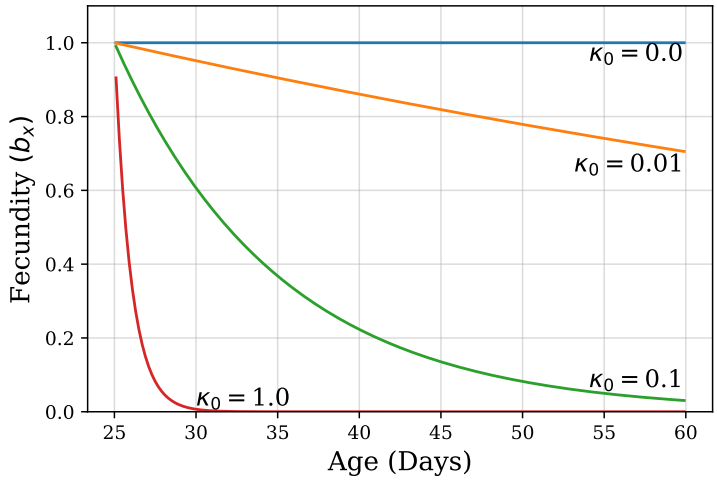

Figure 12: Sensitivity of the fecundity TPC to changes in κ_0.

Figure 13 shows that the TPC shape for κ remains qualitatively the same (for the two meaningful extreme values of κ_0):

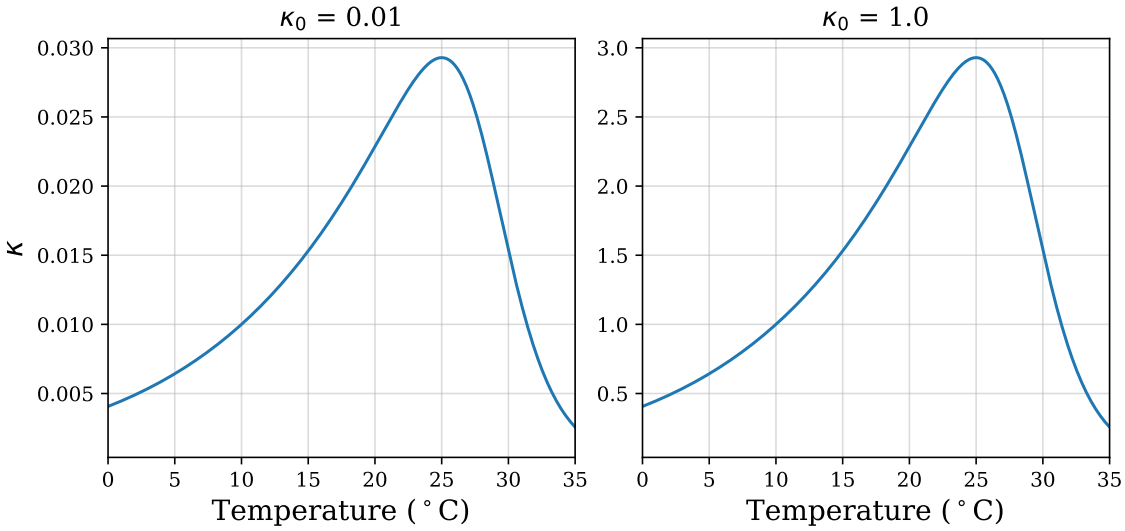

Figure 13: Insensitivity of the κ curve to meaningfully extreme κ_0 values.

2.7.1 Effect on the trait sensitivity results

First, we re-evaluate the trait sensitivity analysis results (Fig. 14). As expected, in the case where baseline kappa (κ_0) is lower, maximum fecundity (b_{max}) becomes more important relative to κ, leaving the order of importance of the 5 traits the same as for the intermediate case (κ_0=0.1) upon which our main results are based.

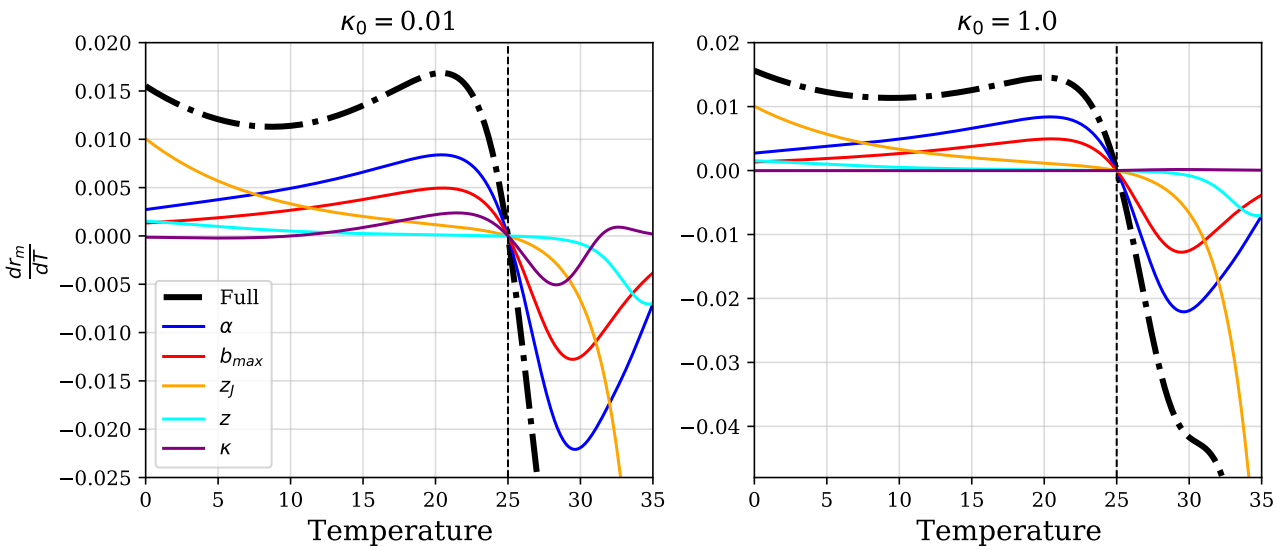

Figure 14: Re-evaluation of the results of the trait sensitivity analysis

2.7.2 The selection gradients revisited

Next we re-evaluate the r_m TPC and selection gradients as above. We focus only on the dominant trait α because the order of the strengths of selection gradients is bound to remain unchanged due to the unchanged order of trait sensitivity irrespective of the κ_0 value (previous section). Figure 15 shows that the selection gradient remains qualitatively unchanged, with overall r_m lower when κ_0 is high, as expected.

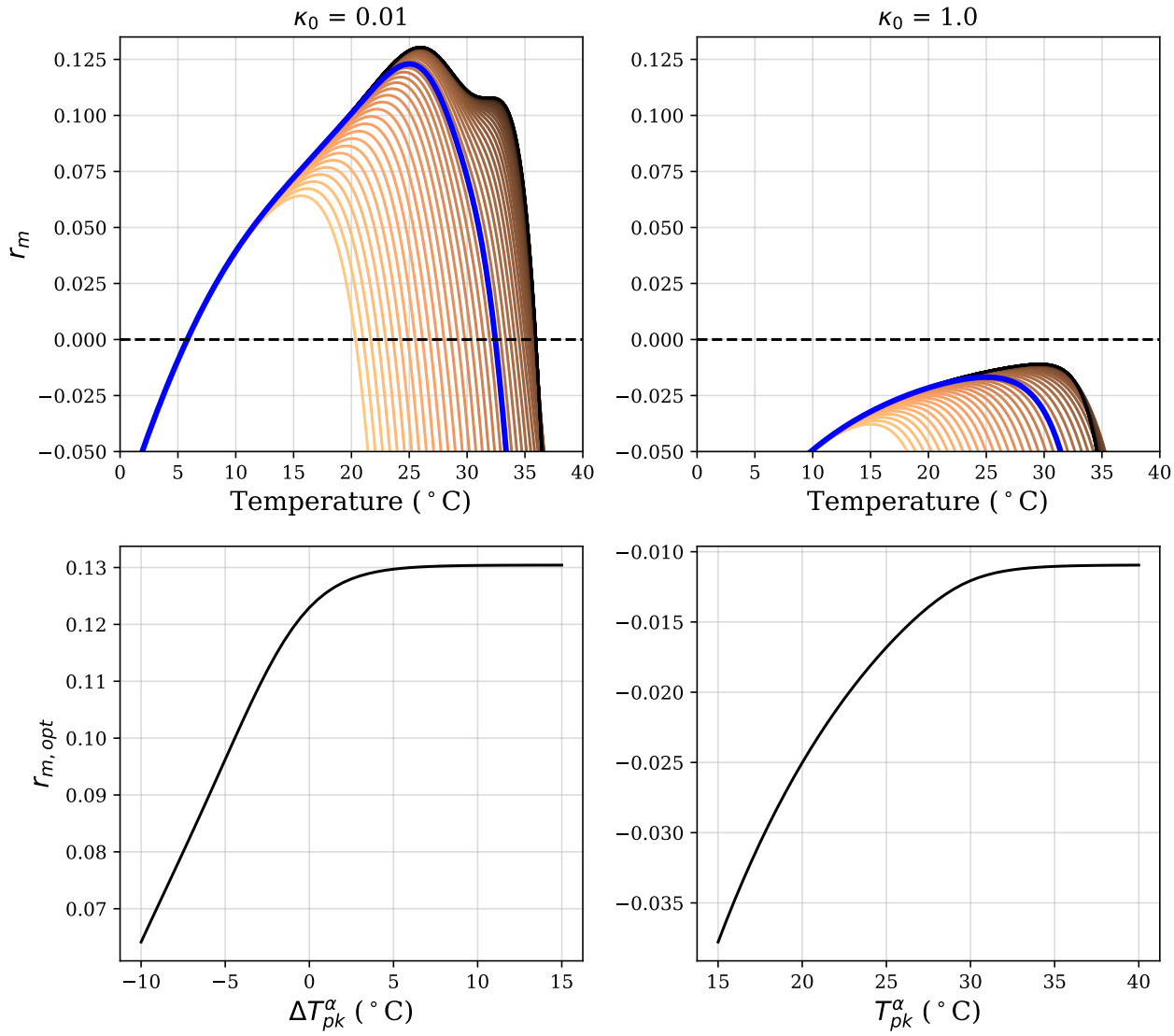

Figure 15: Insensitivity of r_m selection gradient to changes in κ_0

2.8 Macroevolutionary patterns and phylogenetic constraints

The results of our phylogenetic analyses confirm the predicted ordering of T_{pk}s (albeit with wide uncertainty bounds; Fig. 16A), and also reveal differences in phylogenetic structure. Specifically, for T^{α}_{pk}, $T^{b_{max}}_{pk}$, and likely T^{z}_{pk}, closely related species were much more similar than randomly selected species (high phylogenetic heritability; Fig. 16B). This pattern was weaker for $T^{z_J}_{pk}$, suggesting a more pronounced role of plasticity compared to the other T_{pk}s. Moreover, we find evidence that T^{α}_{pk} has evolved more slowly than $T^{b_{max}}_{pk}$ (Fig. 16C). This finding is consistent with the predicted stronger selection on T^{α}_{pk} (Main text).

Our phylogenetic analyses also reveal a significant and strong positively correlated evolution between T^{α}_{pk} and $T^{b_{max}}_{pk}$ (Fig. 16D) in particular. This agrees with the theoretical expectation that fitness increases as mismatches among traits' T_{pk}s are minimized, as these are two most influential traits in terms of their effects on thermal fitness. This finding is notable also because it indicates that across taxa the fitness increase by minimisation of physiological mismatch between these two key traits overrides the effects of energetic allocation constraints and the temperature–size rule, which would predict a weaker or even negative correlation between them. To clarify, warmer temperatures accelerate development, which generally decreases body size. This pattern is known as the temperature–size rule, and partly explains the widely

observed increases in body size with latitude or decreasing temperatures in ectotherms (Bergmann's or James' rule; (43)). Larger body size increases fecundity (increasing fitness), but growing for longer duration increases realised mortality across juvenile stages and reduces the number of generations completed within a year or season (decreasing fitness). Indeed, a growing number of studies have found significant selection on larval development rate to reduce larval mortality and generation time, counterbalancing the positive fitness effect of increasing body size on fecundity (44; 45; 46).

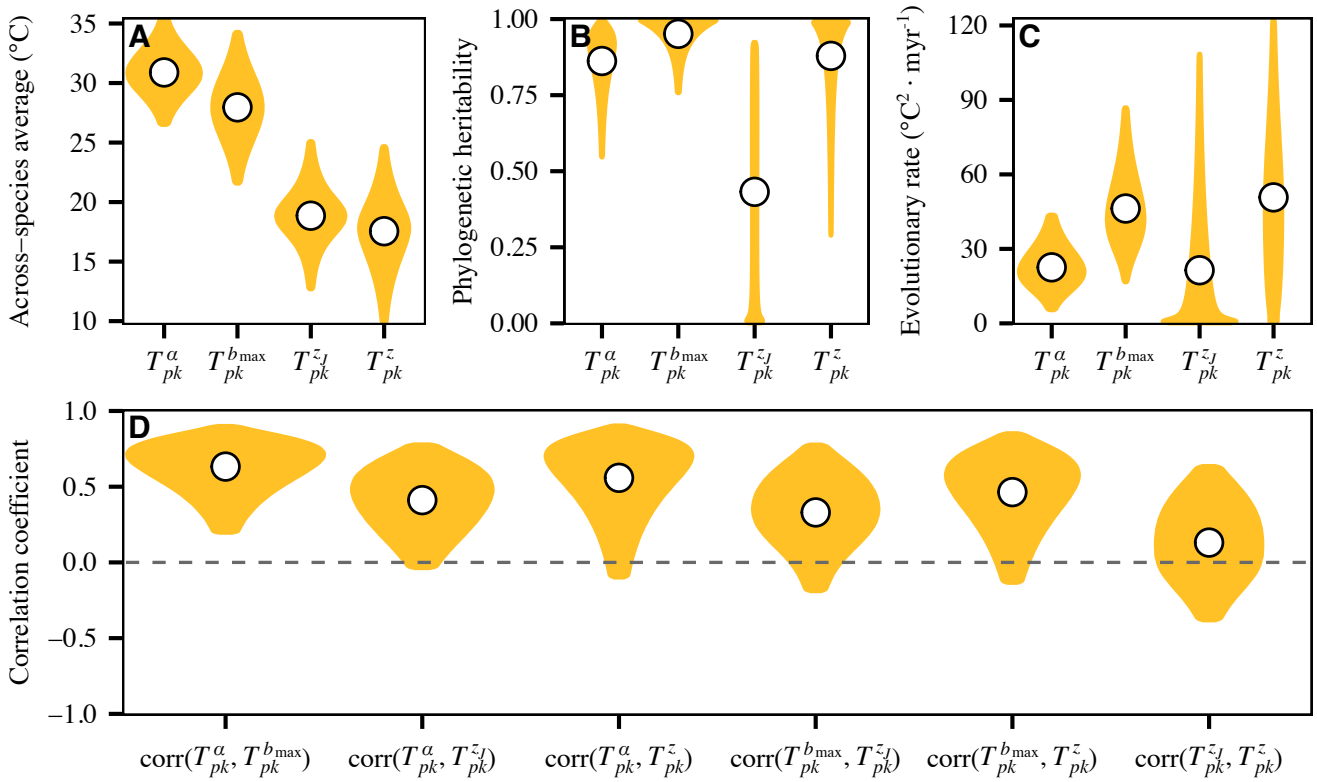

Figure 16: Macroevolutionary patterns of T_{pk}s across arthropods. A: The average T_{pk} values across species, after accounting for evolutionary relationships and for the uncertainty around each T_{pk} estimate. **B:** The fraction of variance in T_{pk} values that is explained by the phylogeny, assuming a Brownian Motion model of trait evolution. The remaining variance arises from phylogenetically-independent sources (e.g., plasticity). **C:** The rate of evolution (under Brownian Motion) per million years. **D:** Correlations between T_{pk} pairs. Gold areas represent the 95% Highest Posterior Density interval for each parameter, as estimated from 100 separate model runs, with 3 replicate chains per run (see Methods). White circles stand for the median.

Table 2: Nucleotide sequences collected for each species from the SILVA (SSU and LSU) and Barcode of Life Data System (COI-5P) databases.

Species	SSU ID	LSU ID	COI-5P ID
Acyrthosiphon pisum	ABLF02002530.1.2075	F02004049.1.2297	-
Aedes aegypti	AAGE02033765.6222.8206	AAGE02025420.70.4046	CULSA016-19
Aedes albopictus	GCLM01041991.604.2545	MNAF02000533.14119.17736	ACMIP154-07
Aedes krombeini	-	-	-
Amblyseius swirskii	-	-	GBMNC68842-20
Amblyseius womersleyi	-	-	GBCH5643-13
Anopheles gambiae	AM157179.1.2015	LCWJ01002898.1.3298	CULSA066-19
Anoplophora glabripennis	-	-	GBMNE15612-21
Antestiopsis thunbergii	-	-	-
Anthonomus grandis	EU215423.9073.11005	EU215423.12455.16248	GBMIN12012-13
Aphis gossypii	-	-	ACEA143-14
Aphis nasturtii	-	-	ACEA530-14
Aubeonymus mariaefranciscae	-	-	-
Bemisia tabaci	GCZW01018184.195.2694	-	BTB002-12
Callosobruchus analis	-	-	GBCCH430-13
Callosobruchus chinensis	-	-	CSP030-09
Callosobruchus maculatus	GEUE01061439.889.2802	GEUD01155100.99.2572	GBCCH431-13
Callosobruchus rhodesianus	-	-	GBCL2570-06
Clavigralla tomentosicollis	GAJX01000019.410.2325	-	GBMNA17782-19
Culex annulirostris	-	-	GBMNC791-20
Culex pipiens	AY988445.1.1858	-	CULSA020-19
Culex quinquefasciatus	AAWU01003351.41983.43837	AAWU01047416.6583.8759	GBDP12712-12
Drosophila suzukii	AWUT01011932.32096.34063	AWUT01017126.2.3394	GBDPD245-14
Gastrolina depressa	-	-	GBMNA17939-19
Halyomorpha halys	GEDY01000115.149.2061	GBHT01004590.7.2044	AGIRI147-17
Harmonia axyridis	KP419116.1.1832	-	GBCL17655-14
Helicoverpa armigera	KT343378.1.1903	-	GBGL29849-19
Hylobius transversovittatus	-	-	GBCL3480-08
Iphiseius degenerans	-	-	TZBCA378-07
Kampimodromus aberrans	-	-	-
Laricobius nigrinus	KP419143.1.1857	-	GBCL9856-12
Leptinotarsa decemlineata	GEEF01054810.5881.7790	-	FBCOP312-13
Macrocentrus iridescens	-	-	BBHEC285-09
Macrosiphum euphorbiae	-	-	ACEA250-14
Monochamus leuconotus	-	-	-
Muscidifurax raptorellus	-	-	-
Muscidifurax zaraptor	-	-	-
Myzus persicae	LXJY01000320.20922.22509	-	GBMNE22299-21
Otiorhynchus sulcatus	AF250084.1.1795	-	COLFD838-12
Paracoccus marginatus	FIZT01020513.6507.8206	-	GBMIN46559-16
Phenacoccus solenopsis	-	-	GBMHH29894-19
Planococcus citri	GAXF02029206.892.3340	-	GBMIN46549-16
Plutella xylostella	AHIO01004014.23148.25041	-	AACTA1852-20
Rhopalosiphum maidis	-	-	ACEA794-14
Sepedon spinipes	-	-	FIDIP848-12
Stethorus punctillum	EF512328.1.1788	-	ASCMT030-11
Tetraneura nigriabdominalis	-	-	ASHMT220-11
Tetranychus evansi	AB926295.1.1858	-	GACAC126-12
Tetranychus mcdanieli	-	-	-
Tetranychus urticae	CAEY01001788.15245.16831	AY750693.1.2826	GACAC6465-19
Thrips hawaiiensis	-	-	AGIMP052-16
Tribolium castaneum	HM156711.1.1831	-	BIPR011-13
Trichogramma bruni	-	-	-
Trichogramma sp. nr. *Lutea*	-	-	KMPUH785-19

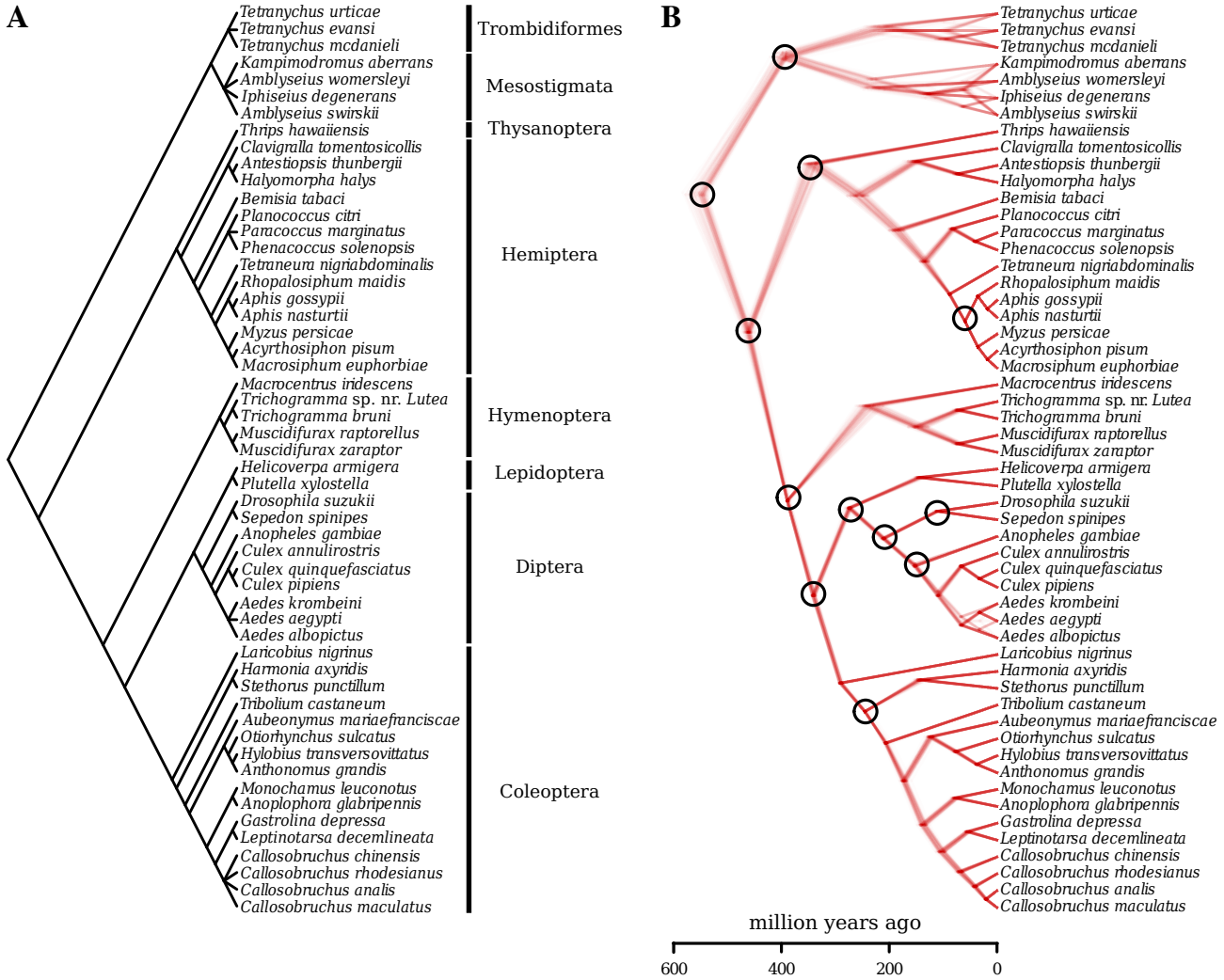

Figure 17: A: The Open Tree of Life topology for the species in the study, with orders explicitly shown. Note that this topology includes some polytomies (e.g., see the *Callosobruchus* and *Tetranychus* clades). B: The final set of 100 time-calibrated trees overlaid on top of each other. Differences in both topology and branch lengths can be observed. Some polytomies from panel A were objectively resolved (e.g., the *Callosobruchus* clade) based on the concatenated sequence alignment. In contrast, where sequence data were completely missing for at least one species (e.g., the *Tetranychus* clade), polytomies were randomly resolved. Nodes whose age was obtained from the TimeTree database are marked with a circle. The two panels were plotted with the ape (47) (v.5.6-2) and phytools R packages (48) (v.1.2-0), respectively.

References

[1] E. L. Charnov, *Life history invariants: some explorations of symmetry in evolutionary ecology* (Oxford University Press, Oxford England, 1993).

[2] V. M. Savage, *et al.*, Effects of body size and temperature on population growth, *Am. Nat.* **163**, 429–41 (2004).

[3] P. Amarasekare, V. Savage, A framework for elucidating the temperature dependence of fitness, *Am. Nat.* **179**, 178–91 (2012).

[4] L. J. Cator, *et al.*, The role of vector trait variation in vector-borne disease dynamics, *Front. Ecol. Evol.* **8**, 189 (2020).

[5] R. Schoolfield, P. Sharpe, C. Magnuson, Non-linear regression of biological temperature-dependent rate models based on absolute reaction-rate theory, *J. Theor. Biol.* **88**, 719–731 (1981).

[6] D.-G. Kontopoulos, *et al.*, Phytoplankton thermal responses adapt in the absence of hard thermodynamic constraints, *Evolution* **74**, 775–790 (2020).

[7] A. I. Dell, S. Pawar, V. M. Savage, Systematic variation in the temperature dependence of physiological and ecological traits, *Proc. Natl. Acad. Sci. U. S. A.* **108**, 10591–10596 (2011).

[8] P. K. P. Molnár, S. J. S. Kutz, B. M. B. Hoar, A. P. A. A. P. Dobson, Metabolic approaches to understanding climate change impacts on seasonal host-macroparasite dynamics, *Ecol. Lett.* **16**, 9–21 (2013).

[9] P. J. Huxley, K. A. Murray, S. Pawar, L. J. Cator, The effect of resource limitation on the temperature dependence of mosquito population fitness, *Proc. R. Soc. B* **288**, rspb.2020.3217 (2021).

[10] E. Mordecai, *et al.*, Optimal temperature for malaria transmission is dramatically lower than previously predicted, *Ecol. Lett.* **16**, 22–30 (2013).

[11] P. Amarasekare, R. Sifuentes, Elucidating the temperature response of survivorship in insects, *Funct. Ecol.* **26**, 959–968 (2012).

[12] T. M. Lunde, M. N. Bayoh, B. Lindtjørn, How malaria models relate temperature to malaria transmission., *Parasit. Vectors* **6** (2013).

[13] T. Van der Have, A proximate model for thermal tolerance in ectotherms, *Oikos* **98**, 141–155 (2002).

[14] D. A. Asbury, M. J. Angilletta, Thermodynamic effects on the evolution of performance curves, *Am. Nat.* **176**, E40–E49 (2010).

[15] J. G. Kingsolver, The well-temperatured biologist, *Am. Nat.* **174**, 755–768 (2009).

[16] M. J. Angilletta Jr, *Thermal adaptation: a theoretical and empirical synthesis* (Oxford University Press, 2009).

[17] H. Caswell, *Matrix population models* (Sinauer Associates Associates, Inc., Massachusetts, Massachusetts, 1989).

[18] W. D. Hamilton, The moulding of senescence by natural selection, *J. Theor. Biol.* **12**, 12–45 (1966).

[19] A. Rohatgi, Webplotdigitizer: Version 4.5 (2021).

[20] D. Padfield, H. O'Sullivan, S. Pawar, rtpc and nls. multstart: a new pipeline to fit thermal performance curves in r, *Methods in Ecology and Evolution* **12**, 1138–1143 (2021).

[21] P. J. Huxley, K. A. Murray, S. Pawar, L. J. Cator, Competition and resource depletion shape the thermal response of population fitness in *Aedes aegypti*, *Commun. Biol* **5**, 1–11 (2022).

[22] C. E. Hinchliff, *et al.*, Synthesis of phylogeny and taxonomy into a comprehensive tree of life, *Proceedings of the National Academy of Sciences* **112**, 12764–12769 (2015).

[23] F. Michonneau, J. W. Brown, D. J. Winter, rotl: an R package to interact with the Open Tree of Life data, *Methods in Ecology and Evolution* **7**, 1476–1481 (2016).

[24] S. Ratnasingham, P. D. N. Hebert, BOLD: The Barcode of Life Data System (http://www.barcodinglife.org), *Molecular Ecology Notes* **7**, 355-364 (2007).

[25] C. Quast, *et al.*, The SILVA ribosomal RNA gene database project: improved data processing and web-based tools, *Nucleic Acids Research* **41**, D590–D596 (2012).

[26] K. Katoh, D. M. Standley, MAFFT multiple sequence alignment software version 7: improvements in performance and usability, *Molecular Biology and Evolution* **30**, 772–780 (2013).

[27] K. Katoh, H. Toh, Improved accuracy of multiple ncRNA alignment by incorporating structural information into a MAFFT-based framework, *BMC Bioinformatics* **9**, 1–13 (2008).

[28] A. W. M. Dress, *et al.*, Noisy: identification of problematic columns in multiple sequence alignments, *Algorithms for Molecular Biology* **3**, 7 (2008).

[29] D. Darriba, *et al.*, ModelTest-NG: a new and scalable tool for the selection of DNA and protein evolutionary models, *Molecular Biology and Evolution* **37**, 291–294 (2020).

[30] T. Flouri, *et al.*, The phylogenetic likelihood library, *Systematic Biology* **64**, 356–362 (2015).

[31] N. Sugiura, Further analysis of the data by Akaike's information criterion and the finite corrections, *Communications in Statistics - Theory and Methods* **7**, 13–26 (1978).

[32] A. M. Kozlov, D. Darriba, T. Flouri, B. Morel, A. Stamatakis, RAxML-NG: a fast, scalable and user-friendly tool for maximum likelihood phylogenetic inference, *Bioinformatics* **35**, 4453–4455 (2019).

[33] S. Kumar, *et al.*, TimeTree 5: An Expanded Resource for Species Divergence Times, *Molecular Biology and Evolution* **39**, msac174 (2022).

[34] J. M. Eastman, L. J. Harmon, D. C. Tank, Congruification: support for time scaling large phylogenetic trees, *Methods in Ecology and Evolution* **4**, 688–691 (2013).

[35] M. W. Pennell, *et al.*, geiger v2.0: an expanded suite of methods for fitting macroevolutionary models to phylogenetic trees, *Bioinformatics* **30**, 2216–2218 (2014).

[36] S. A. Smith, B. C. O'Meara, treePL: divergence time estimation using penalized likelihood for large phylogenies, *Bioinformatics* **28**, 2689–2690 (2012).

[37] J. D. Hadfield, MCMC Methods for Multi-Response Generalized Linear Mixed Models: The MCMCglmm R Package, *Journal of Statistical Software* **33**, 1–22 (2010).

[38] J. Hadfield, S. Nakagawa, General quantitative genetic methods for comparative biology: phylogenies, taxonomies and multi-trait models for continuous and categorical characters, *Journal of Evolutionary Biology* **23**, 494–508 (2010).

[39] P. de Villemereuil, S. Nakagawa, *Modern Phylogenetic Comparative Methods and Their Application in Evolutionary Biology: Concepts and Practice*, L. Z. Garamszegi, ed. (Springer, 2014), pp. 287–303.

[40] V. M. Savage, E. J. Deeds, W. Fontana, Sizing up allometric scaling theory, *PLoS computational biology* **4**, e1000171 (2008).

[41] M. Frazier, R. B. Huey, D. Berrigan, Thermodynamics constrains the evolution of insect population growth rates:"warmer is better", *Am. Nat.* **168**, 512–520 (2006).

[42] S. Pawar, A. I. Dell, V. M. Savage, J. L. Knies, Real versus Artificial Variation in the Thermal Sensitivity of Biological Traits, *Am. Nat.* **187**, E41–E52 (2016).

[43] L. B. Buckley, J. G. Kingsolver, Evolution of thermal sensitivity in changing and variable climates, *Annu. Rev. Ecol. Evol. Syst.* **52**, 563–586 (2021).

[44] D. J. Eck, R. G. Shaw, C. J. Geyer, J. G. Kingsolver, An integrated analysis of phenotypic selection on insect body size and development time, *Evolution* **69**, 2525–2532 (2015).

[45] X.-L. Huang, L. Xiao, H.-M. He, F.-S. Xue, Effect of rearing conditions on the correlation between larval development time and pupal weight of the rice stem borer, Chilo suppressalis, *Ecology and Evolution* **8**, 12694–12701 (2018).

[46] E. Chirgwin, K. Monro, Correlational selection on size and development time is inconsistent across early life stages, *Evolutionary Ecology* **34**, 681–691 (2020).

[47] E. Paradis, K. Schliep, ape 5.0: an environment for modern phylogenetics and evolutionary analyses in R, *Bioinformatics* **35**, 526-528 (2019).

[48] L. J. Revell, phytools: an R package for phylogenetic comparative biology (and other things), *Methods in Ecology and Evolution* **3**, 217–223 (2012).